



NRL/MR/7330--10-9271

Validation Test Report for GDEM4

MICHAEL CARNES

*Ocean Sciences Branch
Oceanography Division*

ROBERT W. HELBER

CHARLIE N. BARRON

JAN M. DASTUGUE

*Ocean Dynamics and Prediction Branch
Oceanography Division*

August 19, 2010

Approved for public release; distribution is unlimited.

REPORT DOCUMENTATION PAGE				<i>Form Approved OMB No. 0704-0188</i>	
Public reporting burden for this collection of information is estimated to average 1 hour per response, including the time for reviewing instructions, searching existing data sources, gathering and maintaining the data needed, and completing and reviewing this collection of information. Send comments regarding this burden estimate or any other aspect of this collection of information, including suggestions for reducing this burden to Department of Defense, Washington Headquarters Services, Directorate for Information Operations and Reports (0704-0188), 1215 Jefferson Davis Highway, Suite 1204, Arlington, VA 22202-4302. Respondents should be aware that notwithstanding any other provision of law, no person shall be subject to any penalty for failing to comply with a collection of information if it does not display a currently valid OMB control number. PLEASE DO NOT RETURN YOUR FORM TO THE ABOVE ADDRESS.					
1. REPORT DATE (DD-MM-YYYY) 19-08-2010		2. REPORT TYPE Memorandum Report		3. DATES COVERED (From - To)	
4. TITLE AND SUBTITLE Validation Test Report for GDEM4				5a. CONTRACT NUMBER	
				5b. GRANT NUMBER	
				5c. PROGRAM ELEMENT NUMBER 0603207N	
6. AUTHOR(S) Michael R. Carnes, Robert W. Helber, Charlie N. Barron, and Jan Dastugue				5d. PROJECT NUMBER	
				5e. TASK NUMBER	
				5f. WORK UNIT NUMBER 73-5091-K0-5	
7. PERFORMING ORGANIZATION NAME(S) AND ADDRESS(ES) Naval Research Laboratory Oceanography Division Stennis Space Center, MS 39529-5004				8. PERFORMING ORGANIZATION REPORT NUMBER NRL/MR/7330--10-9271	
9. SPONSORING / MONITORING AGENCY NAME(S) AND ADDRESS(ES) Space & Naval Warfare Systems Command 2451 Crystal Drive Arlington, VA 22245-5200				10. SPONSOR / MONITOR'S ACRONYM(S) SPAWAR	
				11. SPONSOR / MONITOR'S REPORT NUMBER(S)	
12. DISTRIBUTION / AVAILABILITY STATEMENT Approved for public release; distribution is unlimited.					
13. SUPPLEMENTARY NOTES					
14. ABSTRACT Since the 1970s, the U.S. Navy has maintained a state-of-the-art gridded global monthly full-depth climatology of temperature and salinity and their standard deviations called the Generalized Digital Environmental Model (GDEM). The present document describes the development and evaluation of GDEM4, the newest version of GDEM. As part of the evaluation of GDEM4, comparisons are made in this report to GDEM3 and to four other ocean climatologies: the NODC World Ocean Atlas (WOA2005), the NODC 1/4 degree resolution climatology, the WOCE Global Hydrographic Climatology (WGHC), and the NRLMODAS 2D (MODAS2D) surface temperature climatology. GDEM4 combines the methodology originally developed for GDEM3 with an expanded observation data set. In the evaluations performed, the GDEM4 climatology has been shown to be a significant improvement over GDEM3 and to compare favorably and in many ways improve on fields from the other climatologies used in the evaluations.					
15. SUBJECT TERMS Global ocean climatology Physical oceanography Temperature and salinity observations					
16. SECURITY CLASSIFICATION OF:			17. LIMITATION OF ABSTRACT	18. NUMBER OF PAGES	19a. NAME OF RESPONSIBLE PERSON
a. REPORT	b. ABSTRACT	c. THIS PAGE			Michael Carnes
Unclassified	Unclassified	Unclassified	UL	62	19b. TELEPHONE NUMBER (include area code) (228) 688-5648

Contents

1	Introduction.....	1
2	Bathymetry.....	2
3	Data Preparation.....	3
4	Horizontal Gridding.....	4
5	Vertical Gradient Correction.....	7
6	Filling underground and over land.....	10
6.1	Approach.....	10
6.2	Single-layer median-value extrapolation (SLMVE).....	11
6.3	Multi-level-dependent extrapolation (MLDE).....	11
7	Comparisons between GDEM4 and GDEM3 gridded fields.....	12
7.1	Temperature and salinity differences.....	13
7.2	Temperature and salinity standard deviation comparisons.....	15
8	Conclusions.....	18
9	References.....	20
10	Tables.....	23
11	Figures.....	25

1 Introduction

Since the 1970's, the U.S. Navy has maintained a state-of-the-art gridded monthly full-depth climatology of temperature and salinity and their standard deviations called the Generalized Digital Environmental Model (GDEM). The history of GDEM, originally developed at the Naval Oceanographic Office including the current GDEM-V 3, is documented in Carnes (2009). The earlier GDEM-V 2 is described in Teague et al. (1990). The present document describes the development and evaluation of GDEM 4 (to be called GDEM4 in this report), the newest version of GDEM. The "V" used in the names prior to version 4 indicated that the horizontal resolution was variable. However, since version 4 uses constant horizontal spacing between nodes of the global grid, the suffix "V" has been dropped from the name.

As part of the evaluation of GDEM4, comparisons are made in this report to GDEM3 and to four other ocean climatologies: the NODC World Ocean Atlas (WOA2005), the NODC $\frac{1}{4}^\circ$ -resolution climatology, the WOCE Global Hydrographic Climatology (WGHC), and the NRL MODAS 2D (MODAS2D) surface temperature climatology.

The global World Ocean Atlases produced by the National Oceanographic Data Center have become the standard for ocean climatologies. Since their first climatology produced in 1982, upgraded versions of the climatology were released in 1994, 2001, and 2005. However, the $1^\circ \times 1^\circ$ (latitude, longitude) resolution of these climatologies is inadequate in some regions, particularly near shore and in small seas such as the Sea of Japan, the Mediterranean, and the Persian Gulf. In the present study, we will compare GDEM4 temperature and salinity standard deviations to those from WOA2005 (Locarni et al., 2006 and Antonov et al., 2006).

The NODC WOA2001 $\frac{1}{4}^\circ$ degree climatology (Boyer et al., 2005) is the only other monthly global ocean climatology (besides GDEM3 and GDEM4) with $\frac{1}{4}^\circ$ resolution (or higher). Version 2 of this climatology, which was released in 2003 will be referred to as WOA2001Q2. The quarter-degree climatology was computed by an objective analysis that used the same profile data set as WOA2001 (Stephens et al., 2002; Boyer et al., 2002), and used the WOA2001 1° -resolution fields as the first guess.

The WOCE Global Hydrographic Climatology (WGHC) (Gouretski and Koltermann, 2004) provides global annual average grids of temperature and salinity and their standard deviations at a geographical resolution of 0.5° . They used only profiles having both temperature and salinity. The final gridded fields were computed by optimum interpolation at 45 standard depth levels between the surface and 6000 m. However, the interpolation was performed using profiles previously averaged on isopycnal surfaces within square 55-km boxes. Gouretski and Koltermann (2004) provided no information on the method used to compute standard deviations.

The MODAS2D surface temperature climatology (Kara et al., 2009) was constructed from 15 years of satellite MCSST observations on a global $1/8^\circ$ uniform grid. Daily global surface temperature grids were first computed for each day from 1993 to 2008 by optimum interpolation using all available AVHRR nonlinear SST observations processed by the Naval Oceanographic Office. Monthly averages were then computed at each grid point over the entire multi-year time span, and then monthly grids of standard deviation were computed using the anomalies of the daily grid from the monthly averages.

2 Bathymetry

The GDEM4 $1/4^\circ$ -resolution bathymetry was derived from the NRL DBDB2 v3.0 global 2-minute-resolution bottom topography (Ko, 2009). It is a composite of the Smith and Sandwell (1997) global seafloor topography in deep water merged with several other high-resolution data sets. It was compared to other topographies in Marks and Smith (2006).

The GDEM4 bathymetry bottom depth at each grid point on the $1/4^\circ \times 1/4^\circ$ global grid was derived as the deepest bottom depth contained within the 9 (or 10) \times 9 (or 10) 2-minute-resolution grid subset from DBDB2 centered at the GDEM4 grid node. The procedure uses 9 values (length of 0.27 degrees) on one side when the GDEM4 $1/4^\circ$ and the DBDB2 $1/30^\circ$ grid nodes coincide at whole and half geographic degree locations, and 10 values are used when the GDEM4 location is centered between two DBDB2 grid nodes. The 10-point DBDB2 subgrid side (to the center of the end cells) is 18 minutes (or 0.3 degrees) long and the 9-point DBDB2 side is 16 minutes (or 0.27 degrees) long as compared to the 0.25 degree GDEM4 grid cell size. As a result, the GDEM4 bottom depths carve out deeper segments of the bottom than the higher-resolution DBDB2 bathymetry. In addition, along sloping bathymetry and at the surface, the GDEM bathymetry cuts into the land edges, sometimes cutting through narrow land bridges.

The GDEM3 bathymetry was derived by regridding the NAVO DBDB5 5-minute-resolution global bathymetry using bi-linear interpolation. The difference (GDEM4-GDEM3) between the subsurface GDEM4 and the GDEM3 depths, both on the same $1/4^\circ$ grids, is shown on the global map in Figure 1. The depth differences range from negative 2911 m to positive 3844 m, but the color range in this figure is restricted to ± 1000 m to highlight the mid range of differences. The mean global difference is 119 m with a standard deviation of 249 m. The greater average depth of GDEM4 is expected because its depths were derived as the greatest depth from DBDB2 within each grid cell boundary whereas the GDEM3 depths were computed by interpolation from the four surrounding DBDBV 5 depths. The depth differences in the Persian Gulf and the Yellow Sea are shown in Figures 2a and 2b, respectively. The range of the color scale is the same for each (-20 m to 50 m). The largest differences usually occur where bottom gradients are largest, but sometimes are seen in the relatively flat and shallow plains near the boundaries. GDEM values are computed only at the subset of the 78 standard depths (listed at the end of Section 3 below) above or at the bottom bathymetry depth at each grid location, so that in most cases, the deepest GDEM value is computed at a standard depth above the bottom. However, as discussed in Section 6, there is filled version of

GDEM in which all values are extrapolated down to 6600 m depth, and the user can then truncate GDEM profiles at any location to any desired depth down to 6600 m.

3 Data Preparation

The temperature and salinity profile dataset used in the calculation of the GDEM4 climatology was constructed by combining profiles from the Navy's MOODS (Master Oceanographic Observation Data Set) profile archive (Bauer, 1982; Jugan and Beresford, 1991) with classified profiles removed, the WOD 2005 (World Ocean Database) (Boyer et al., 2006), and delayed-mode Apex profiles downloaded from the USGODAE server (www.usgodae.org/argo/argo.html) on October 11, 2007. Palace and Apex profiles in were first removed from MOODS and WOD 2005. Then, a duplicate check was performed that removed any profiles from MOODS that appeared in the WOD 2005 data set. The final combined data set consisted of 8,302,197 profiles. The number of profiles measured by each of 33 different categories of instruments is listed in the second column of Table 2. The first column of Table 2 is an instrument code number (used in MOODS) that is defined, in terms of instrument type description, in Table 2.

The full data set of profiles was examined using a GUI-based editor. The editor displayed all profiles in geographical blocks up to 10° of latitude by 10° of longitude in size. Smaller subsets of profiles, grouped by position and time of year within the largest block, could be examined in an automated sequence of profile overlays of temperature versus depth, salinity versus depth, potential density versus depth, potential density versus salinity, temperature versus potential density, and salinity versus potential density. Outliers on each plot could then be easily identified and then marked for deletion by the operator. The editing GUI also allowed profiles to be individually edited, but this capability was not used often due to the large amount of time required if applied to the full data set. Not counting profiles measured by MBT, moored buoys, or drifting buoy, the manual editing identified and removed 692,739 profiles. The MBT, moored buoy, and drifting buoy observations were then removed together with all profiles having only one or two observations each. The MBT observations were removed due to the low precision and accuracy, short maximum depth (maximum of 285 m, but often much less), and questionable quality. The number of profiles of each measurement type in this first set of deletions is listed in Table 1. Altogether, 3,621,099 (43.6% of the total) profiles were deleted from the database up to this point. Next, all profiles where the deepest observation depth was less than 200 m, but the bottom bathymetry depth was greater than 400 m were removed. This step removed another 268,442 (3.2 % of the original total) profiles. The final data set contained 4,412,454 temperature profiles and 1,969,081 salinity profiles distributed among the various instrument types as shown in columns 6 and 7 of Table 1. The GDEM3 climatology was constructed from 1,732,013 temperature and 998,225 salinity profiles.

The geographical distribution of temperature and salinity profiles are displayed in Figures 3 and 4, respectively, as the \log_{10} of the number of profiles within each 10° x 10° geographic block. The distribution of profiles in terms of their year of measurement is shown in Figure 5. Because the MBTs were eliminated from the final data set, the

number of temperature and salinity profiles is about equal in the years before 1960, but after XBTs began to be used in the 1960s, the number of temperature-only profiles far outnumbered profiles with both temperature and salinity. The relative number of profiles with both temperature and salinity has been steadily rising since the late 1990s due to the use of Palace and Apex floats in deep water.

The final step in the preparation of the profile data set interpolated each profile to a set of 78 fixed depths between 0 m and 6800 m using the piece-wise cubic interpolating polynomial interpolator, similar to the pchip interpolating method in MATLAB and GNU OCTAVE. The advantage of the pchip technique is that over intervals of the original data that are monotonically increasing or decreasing, the interpolated curve is also monotonic in the same direction. Also, the interpolated curve contains local extremes only at points where the original data do. As a result, overshoots that might occur with splines near sudden gradient changes in the original data are eliminated.

The Arctic Ocean presented a special challenge due to the very low number of observations available. Our approach was to prepare the Arctic monthly climatologies separately from those for the rest of the world, and then splice the two parts (Arctic and non-Arctic) together at the end. The sparse data set in the Arctic was supplemented by using synthetic profiles extracted from the Polar science center Hydrographic Climatology (PHC) version 3.0 (Steele et al., 2001). The PHC 3.0 is a global $1^\circ \times 1^\circ$ resolution global climatology in which the NODC WOA 1998, the Environmental Working Group (EWG) Arctic Ocean Atlas (AOA), and Canadian data provided by the Bedford Institute of Oceanography were merged by optimum interpolation. The EWG (Arctic Climatology Project, 1997, 1998) was produced in a joint project between Russia and the U.S that used more than one million observations collected from Russian drifting stations, ice breakers and airborne expeditions plus U.S. buoy observations declassified for this project. The Russian observations were not released to the public, so instead we used the PHC 3.0, with the EWG climatology imbedded in it, as a substitute. A decimated set of temperature and salinity profiles were extracted from each monthly PHC climatology. Profiles from the 1° resolution PHC climatology at positions from 64° N to the pole, but from 51° N to the pole in the vicinity of Hudson Bay, were extracted at latitude intervals of 1 degree and at longitude intervals of $0.45/\cos(\text{latitude})$ degrees (but at intervals of at least 1 degree). The extracted profiles were interpolated to the 78 standard depths of the GDEM4 climatology. The 78 GDEM4 standard depths are: every 2 m from 0 m to 10 m, every 5 m from 10 m to 100 m, every 10 m from 100 m to 200 m, every 20 m from 200 m to 300 m, every 50 m from 300 m to 500 m, every 100 m from 400 m to 1800 m, and every 200 m from 1800 m to 6600 m.

4 Horizontal Gridding

The climatology for each month of the year was produced by first gridding the observations on each depth surface over the entire domain. A second step then adjusted the vertical structure of the gridded result to better match the vertical gradient of the

observations. A final step adjusts the vertical structure of both temperature and salinity to ensure that each profile is statically stable.

The horizontal gridding of profile values or coefficients in versions of GDEM prior to version 3 (Teague et al., 1990) was performed using the minimum curvature method (Briggs, 1974; Swain, 1976). Smith and Wessel (1990) later showed that this technique might produce large erroneous oscillations, particular in data-sparse regions of the interpolated grid. They also showed that adding a tension term to the interpolation equations could eliminate such oscillations. The minimum curvature technique was shown by Panteleev and Yaremchuk (1989) and Panteleev and Filyushkin (1995) to be preferable to optimal interpolation unless the covariance length scales of the data being gridded are known accurately. The interpolation equations for a discrete grid are derived by simultaneously minimizing, with respect to each gridded value, the squared difference between the observations and the gridded values (minimizing the data error) plus the squared second derivative of the gridded quantity (minimizing the curvature), with respect to the coordinate values. The tension term is added by also minimizing the squared first derivative of the gridded values (minimizing the slopes). This technique was used by Brasseur et al. (1996) to grid temperature and salinity in a finite element context to produce the Mediterranean Oceanic DataBase (MODB). Experiments leading to the development of the GDEM3 climatology determined that a robust approach was obtained by retaining the slope minimization term and eliminating the curvature minimization term. Therefore, the gridding equations were derived by minimizing the squared slope and data misfit to the final gridded value,

$$J = \sum_m \sum_n \left\{ \left(\frac{T_{n+1,m} - T_{n,m}}{\Delta x_m / \Delta y} \right)^2 + \left(\frac{T_{n,m+1} - T_{n,m}}{1} \right)^2 + F \sum_k (T_{m,n} - \theta_{m,n,k})^2 \right\} \quad (1)$$

(for all n,m grid points not over land) with respect to each grid value ($T_{i,j}$). Each $T_{n,m}$ is the final gridded value at the n,m grid indexes, where n is the east-west index and m is the north-south index. $\theta_{n,m,k}$ is the kth observed value within $\frac{1}{2}$ grid cell width and height from the (n,m) grid node. The grid cell meridional length, Δy (27.7 km for the $\frac{1}{4}$ grid), is a constant, but the zonal length narrows toward the poles, $\Delta x_m = \Delta y \cos(\lambda)$, where λ is the latitude in radians. The grid-resolution-independent factor, $F = 1$, was chosen by experimentation to balance smoothness with resolution. A smaller value, $F = 1/15$, was chosen for gridding the variance data (squared anomalies) to produce smoother final fields. The result of the minimization is a system of Poisson equations with the equation at each (i,j) grid node given by

$$T_{i,j} = \left(\frac{(\Delta x_j / \Delta y)^2}{2(\Delta x_j / \Delta y)^2 + 2} \right) \left\{ \frac{T_{i+1,j} + T_{i-1,j}}{(\Delta x_j / \Delta y)^2} + \frac{T_{i,j+1} + T_{i,j-1}}{1} - F \sum_k (T_{i,j} - \theta_{i,j,k}) \right\} \quad (2)$$

Zero-gradient boundary conditions were applied along land boundaries at each depth to eliminate gridding over land and across land boundaries, but still allow data values to diffuse around boundaries. The system of Equations (2) is solved using Gauss-Seidel iteration with over-relaxation.

The minimum curvature technique applied to GDEM (Teague, et al., 1990) prior to GDEM3 did not eliminate gridding over land, and resulted in mixing unlike water types separated by narrow land boundaries. The optimum interpolation gridding approach used to generate the NOAA World Ocean Climatologies attempts to produce the same result by grouping profiles within regional polygons on each side of land boundaries, and interpolating the profiles only within each polygon. This is a tedious approach, where polygons must be re-defined at each depth and where interpolation around long and narrow islands or through narrow straits between separate polygons is difficult to accomplish accurately. The method used here for GDEM4 naturally eliminates gridding on and across land by the use of the zero-gradient boundary conditions along land boundaries, ensuring that communication between any grid cell and the data at any other grid cell takes place only by diffusion through a sequence of adjacent grid cells (but not including grid cells over land) connecting them.

The monthly temperature and salinity standard deviation climatologies were computed, by the same techniques as employed for the monthly mean climatologies, but from the anomalies of the observations from the monthly mean climatologies. Once the temperature and salinity mean climatologies were completed for each month, the anomaly of each observation from the monthly means, interpolated to the position and time of each observation, was computed. Then, the squares of the anomalies were gridded at each depth over the globe using the minimum slope technique. Finally the square root of the resulting average squared-anomaly fields was computed to form the monthly standard deviation climatology fields.

The gridding of the temperature, salinity, temperature variance, and salinity variance was performed separately at each of the 78 depth levels. The preferred approach is to perform the gridding on potential density surfaces as was done for the Hydrobase and WOCE (WGHC) climatologies as recommended in Lozier et al. (1994). The WOCE climatology was gridded on constant depth surfaces, but groups of individual profiles within each grid cell were first averaged along potential density surfaces. Averaging of observations (through the gridding procedure) along constant depth or pressure surfaces in areas of sharply sloping isopycnals can produce water masses with profiles of potential temperature-versus-salinity which are uncharacteristic of the local water masses. However, gridding along isopycnal surfaces requires that both temperature and salinity be present on each observed profile (because potential density must be computed from both temperature and salinity), eliminating the use of all XBT profiles. Also, in the vertically-mixed layer near the surface or in well-mixed coastal waters where a constant density surface is nearly vertical, this approach is difficult or impractical to apply. In addition, selection of one set of density surfaces that adequately resolve the vertical structure of the entire ocean or even of some small regions is nearly impossible. For this reason, the Hydrobase and WOCE climatologies do not grid data in shallow water. Because of the difficulties discussed above combined with the requirement to eliminate XBTs when gridding along potential density surfaces, the GDEM4 climatology was generated instead by gridding along constant depth surfaces.

The full set of historical observations was separated according to time of year before the calculation of each one-month climatology. The center day of the year, d_m , of each monthly climatology, is $d_m = (m-0.5)*365.25/12$, where m is the month number. The time span of observations, centered at d_m for each month, was set within five different depth ranges, shown in Table 1, to a minimum of 45 days near the surface to all days of the year at depths below 1200 m. The depth-dependent scheme was designed to restrict the observations to (nearly) the temporal boundaries of each month near the surface, but to compensate for the reduced number of observations as depth increased by expanding time span.

The number of temperature and salinity observations used in the calculation of the climatology within the time span shown in Table 1 within each grid cell at each depth for each month are stored, as part of the GDEM4, in 12 sets of monthly global grids for temperature and for salinity. The number of observations within each cell is stored as the base 10 logarithm of the number in order to reduce the numeric range when producing plots directly from these files. For example, Figure 6 shows global maps prepared from data in these files for the January climatologies of temperature and salinity at the surface, 1000 m, and 4000 m. A cell is blank (uncolored) if there were no observations available within that time span for the January climatology at that depth. Figure 6a (number of temperature observations at the surface in January) indicates that a few cells have over 1000 observations and many have over 100, particularly in the northwest Atlantic and Pacific, but most cells have fewer than 10 observations. There are fewer salinity observations, and most are from Argo floats in the deep ocean. Very few observations are available in the Arctic Ocean, the Canadian Archipelago, and in the Sea of Okhotsk in winter due to ice cover. At 1000 m depth, the number of temperature and salinity observations is nearly equal since most temperature-only measurements, such as xbts, extend down to only about 800 m. Also, the salinity coverage is greater overall at 1000 m than at 0 m due to the wider time range at 1000 m (120 days) than at 0 m (45 days). At 4000 m, the number of observations is very sparse, particularly in the southeast Pacific Ocean.

Figure 7 shows a regional example that includes the Red Sea, Gulf of Oman, Gulf of Aden, Arabian Sea, and Arabian Gulf, of the number of temperature and salinity observations at the surface and at 60 m in August. The density of temperature observations is high, particularly around the Arabian Peninsula, but the salinity observations are sparse at both depths with fewer than four observations in most non-blank cells. The shallow western shelf of the Arabian Gulf is nearly devoid of surface temperature and salinity observations

5 Vertical Gradient Correction

The distribution of observations can change significantly between adjacent depth levels, leading to depth-dependent biases and unrealistic vertical gradients. Biases also result from combining profiles measured by different instruments (XBT profiles end near 200m, 400m, or 800 m, and CTD profiles and hydrocasts end deeper or near the bottom)

or when maximum profile depths are limited to areas of strongly sloping bottom topography. The depth-dependent temporal subsetting for each monthly climatology used in computing the GDEM4 climatology can also result in increased numbers of observations as depth increases. Since each depth level is gridded independently of any other depth level in GDEM4, the different biases that result at each depth level can lead to unrealistic vertical gradients of the final gridded fields. After completing the horizontal gridding the observations along every depth level, the vertical gradient of each vertical profile in the final gridded climatology was corrected by an objective least-squares technique which forces the vertical gradient of each gridded profile toward the gradient estimated from the data while simultaneously minimizing the difference between the original and corrected gridded profile. The corrected profile values, $\hat{T}_k, k = 1, N$, such as temperature or salinity at a particular horizontal grid location is determined by minimizing the cost function

$$J = \sum_{k=1}^N \left(\frac{\hat{T}_k - T_k}{\sigma_k} \right)^2 + \sum_{k=2}^N \left(\frac{\hat{T}_k - \hat{T}_{k-1} - D_k}{\delta_k} \right)^2 \quad (3)$$

with respect to each final value, \hat{T}_k . In Equation (3), T is the uncorrected variable, σ is the gridded standard deviation of the variable, D is the gridded value of the difference in the variable between depth levels k and $k-1$, and δ is the gridded value of the standard deviation of D . The horizontal gridding to compute the grids of D and δ was performed at each depth surface in the same manner as for temperature, salinity, and their standard deviations, except that the data set for constructing the gridded fields of D was the set profile observation differences between consecutive depth level rather than the set of observations from each depth level. Minimization of the cost function in Equation 3 results in a tri-diagonal system of N equations, where the i^{th} equation is

$$\hat{T}_{i-1} \left(\frac{-1}{\delta_i^2} \right) + \hat{T}_i \left(\frac{1}{\sigma_i^2} + \frac{1}{\delta_i^2} + \frac{1}{\delta_{i+1}^2} \right) + \hat{T}_{i+1} \left(\frac{-1}{\delta_{i+1}^2} \right) = \frac{T_i}{\sigma_i^2} + \frac{D_i}{\delta_i^2} + \frac{D_{i+1}}{\delta_{i+1}^2}, \quad i = 2, N-1, \quad (4)$$

and the first (surface) and last (bottom) equations are

$$\hat{T}_1 \left(\frac{1}{\sigma_1^2} + \frac{1}{\delta_2^2} \right) + \hat{T}_2 \left(\frac{-1}{\delta_2^2} \right) = \frac{T_1}{\sigma_1^2} - \frac{D_2}{\delta_2^2}, \quad i = 1 \quad (5)$$

$$\hat{T}_{N-1} \left(\frac{-1}{\delta_N^2} \right) + \hat{T}_N \left(\frac{1}{\sigma_N^2} + \frac{1}{\delta_N^2} \right) = \frac{T_N}{\sigma_N^2} + \frac{D_N}{\delta_N^2}, \quad i = N. \quad (6)$$

Before application of the vertical gradient correction, the temperature and salinity horizontal grids of vertical difference between adjacent depth levels, Dt for temperature and Ds for salinity, were checked for vertical stability and corrected, if required. The temperature and salinity at the $i-1$ and i depth levels spanned by the vertical difference values Dt_i and Ds_i , were first computed as

$$T'_{i-1} = (T_{i-1} + T_i)/2 - Dt_i/2$$

$$T'_i = (T_{i-1} + T_i)/2 + Dt_i/2$$

$$S'_{i-1} = (S_{i-1} + S_i)/2 - Ds_i/2$$

$$S'_i = (S_{i-1} + S_i)/2 + Ds_i/2,$$

where T and S are from the GDEM4 monthly mean climatology (before application of the vertical gradient correction (Equations 4, 5, and 6)). Then, the potential temperature, θ , was computed at the $i-1$ and i depth levels using the reference pressure midway between the depth levels, $Pr_i = (p_i + p_{i-1})/2$, as

$$\begin{aligned}\theta_{i-1} &= \theta(S'_{i-1}, T'_{i-1}, p_{i-1}, Pr_i) \\ \theta_i &= \theta(S'_i, T'_i, p_i, Pr_i),\end{aligned}$$

and the potential density, ρ , was computed at the $i-1$ and i depth levels at the Pr_i reference pressure as

$$\begin{aligned}\rho_{i-1} &= \rho(S'_{i-1}, \theta_{i-1}, Pr_i) \\ \rho_i &= \rho(S'_i, \theta_i, Pr_i).\end{aligned}$$

The squared Brunt-Vaisala frequency (Jackett and McDougall, 1995) was then computed as

$$N^2 = -\frac{g}{(\rho_{i-1} + \rho_i)/2} \frac{(\rho_i - \rho_{i-1})}{(z_i - z_{i-1})}.$$

If N^2 was less than a specified minimum statically stable value, $N_{\min}^2 = 1.5 \times 10^{-7}$, then the salinity difference, Ds_i , was incrementally increased until $N^2 = N_{\min}^2$.

The vertical gradient correction is effective at eliminating the large erroneous near-bottom vertical gradients often evident in climatologies. Figure 8 and Figure 9 show south-to-north vertical section of temperature and salinity, respectively through the middle of the Yellow Sea along 126.6° E in January. Observed profiles in this region in January typically exhibit well-mixed, nearly constant, vertical structure. However, the GDEM4 temperature (Figure 8a) and salinity (Figure 8b) climatologies exhibit erroneous gradients near the bottom before application of vertical-gradient correction. Over a sloping bottom, the asymmetry of profile locations increase as the distance to the bottom decreases, biasing the average when there is a horizontal gradient of temperature or salinity values away from the slope. The temperature and salinity are nearly uniform vertically after correction (Figure 8b and Figure 9b, respectively). Also shown are the GDEM3 and the WOA2005 temperature and salinity vertical sections. The GDEM3 climatology underwent nearly the same vertical gradient correction as GDEM4, and therefore exhibits a vertically-uniform structure. The WOA2001Q2 shows a temperature inversion near 33° N which is compensated by a near-bottom salinity gradient to form a stable density gradient. However, the WOA2001Q2 grids were stabilized using a method similar to that of Jackett and McDougall (1995), indicating that the near-bottom salinity gradient is not real, and was created to compensate the instability caused by the temperature inversion.

A more dramatic case of vertical gradient correction from the eastern Bering Sea shelf and slope east of Bristol Bay in January is shown in Figures 10, 11, and 12. Figures 10 and 11 show west-to-east vertical sections of temperature and salinity along 58° N in the upper 400 m. For the case of the uncorrected vertical gradient of GDEM4 (Figure 10 a and 11 a), the shelf-break front has weak vertical gradients of temperature and salinity in the upper 50-to-100 m depth range, but then change to a strong inverted temperature gradient (temperature increasing downward) and stable salinity gradient near the bottom

over the shelf. Due to the lack of observations near the bottom over the shelf, the gridding procedure pulled in observations near the shelf bottom from the shelf-break frontal region, resulting in an increasingly warm bias as the bottom is approached. Figure 12 shows the groups of profiles observed in the time span from December 15 to January 15 centered at two different locations along the vertical section transect. Figures 12 a and 12 b show the temperature and salinity profiles near the shelf break centered at 188° E where the water depth is about 115 m, and Figure 10 b and 10c show the profiles over the shelf centered at 191° E where the bottom depth is about 65 m. At both locations, most observed temperature and salinity profiles are vertically well-mixed. The GDEM4 corrected and uncorrected profiles and the GDEM3 profiles are also plotted in Figure 12. Contrary to most observed profiles, the uncorrected GDEM4 profiles at both locations have a strong near-bottom gradient as seen in the vertical section plots of Figure 10. The GDEM3 climatology profiles over the shelf break (Figures 12 a and c) appear to match the gradients of minority subset of observed profiles, probably the only profiles available when GDEM3 was computed. After application of the vertical gradient correction to GDEM4, the strong bottom gradient disappears from the temperature and salinity vertical sections (Figures 10 b and 11 b) and from the profile plots (Figure 12).

The final step in the preparation of the monthly gridded climatologies was the adjustment of the temperature and salinity profile at each grid location to produce a statically stable profile. Due to the vertical gradient correction already applied, the number and severity of instabilities were small. Unstable segments on each profile were identified by the negative squared Brunt-Vaisala frequency (Jackett et al., 1995) computed from the temperature and salinity. Once identified, the local temperature and salinity were modified iteratively until a stable profile was produced.

6 Filling underground and over land

6.1 Approach

The global monthly GDEM fields cover the domain above the bottom bathymetry depths derived from the NRL bathymetry. Underground and over land, values of the 3-D grid are undefined. For some applications of the GDEM climatology must be expanded underground to match the grid and bottom depths of that application. The mismatch between the GDEM bathymetry and that of an application may be due to use of a bottom bathymetry different than that used by GDEM or holes resulting from differences in horizontal resolution. In addition, the GDEM fields do not reach the ocean bottom depth at some locations, particularly where data was not available within local bathymetric extremes (holes). One approach, used previously, to extrapolate GDEM to match other bathymetries expanded the GDEM field values outward horizontally, one depth level at a time. The results from this approach were sometimes flawed by unrealistic vertical gradients underground. Another approach expanded the vertical gradient between adjacent depth levels outward. The resulting expanded vertical gradients were then vertically integrated to obtain the underground field values. This approach resulted in

underground fields with reasonable vertical gradients, but the vertical integration of the vertical gradients to recover the field values (temperature or salinity) often resulted in large biases in the field values as distance below the bottom increased. The approach used to fill the GDEM4 grid combines the single-layer value extrapolation and vertical gradient extrapolation techniques. The single-layer extrapolation technique is first described below, then the multi-layer extrapolation technique, which incorporates the single layer technique applied to both the field values and their vertical gradients is introduced.

6.2 Single-layer median-value extrapolation (SLMVE)

The single-layer extrapolation begins with the surface field and then progresses downward filling each depth level before proceeding to the next. At each level, the grid of values is filled using the single-layer median-value extrapolation (SLMVE) technique developed by Dan Fox (NRL). SLMVE begins with the unfilled grid at depth level k , containing values, $T_{n,m,k}$, some of which are undefined or missing. The algorithm checks each grid (n,m) point, $n=1,N$, $m=1,M$. If the value is missing, then it collects the K non-missing value, $T_{i,j,k}$ contained in the box defined by $n-L \leq i \leq n+L$, $m-L \leq j \leq m+L$, surrounding the (n,m) grid point. The value of L is typically 1, resulting in a 3x3 grid of values centered at (n,m) . If $K/L^2 \geq F$, where $F = 0.3$ is typically used, then $T_{n,m,k}$ is replaced with the median of the K values, otherwise it remains set to the missing value indicator value. The entire grid is scanned, repeatedly replacing missing values that pass the test until no missing values remain. As the sequence of iterations continues, the edge of filled values marches inland until either the edge of the grid is reached or filled values marching in from another direction are met. Once completed, the filled values (but not the original values) are smoothed by three passes of a 2-dimensional 3x3 convolution operator (Shapiro, 1970). The weights of the 3x3 convolution operator are 0.25 at the center, 0.124 at the sides, and 0.0625 at the corners.

6.3 Multi-level-dependent extrapolation (MLDE)

The surface values of temperature, $T_{n,m,1}$ (similarly for salinity), are first extrapolated over land using the single-layer median-value extrapolation (SLMVE) technique. At the next deeper depth level, k , the temperature, T , the temperature variance, σ^2 , the temperature difference average between depth levels k and $k-1$, D (introduced in Equation 3), and the temperature difference variance, δ^2 , are filled using the SLMVE method. The (above ground) grids of D and δ^2 are available as part of GDEM4 because they were computed for each monthly climatology and used in the vertical-gradient correction of the above-ground temperature and salinity fields. At each grid node where the temperature value was originally missing (before application of the SLMVE method), a new (final) value of temperature, \hat{T} , is computed by minimizing the following cost function,

$$J = \left(\frac{T_{n,m,k} - \hat{T}_{n,m,k}}{\sigma_{n,m,k}} \right)^2 + \left(\frac{D_{n,m,k} - (\hat{T}_{n,m,k} - T_{n,m,k-1})}{\delta_{n,m,k}} \right)^2. \quad (7)$$

The first term on the right hand side of (7) is the squared difference of the horizontally-extrapolated temperature value and the new (final) temperature value, normalized by the temperature standard deviation (also extrapolated by SLMVE). The second term is the squared difference between the horizontally-extrapolated average temperature difference, between the k and k-1 levels, and temperature difference between the new temperature (at level k) and the horizontally-extrapolated (or original) temperature value at level k-1, all normalized by the extrapolated temperature difference standard deviation.

Minimizing (7) with respect to the new $\hat{T}_{n,m,k}$ being sought, results in,

$$\hat{T}_{i,j,k} = \frac{\delta_{n,m,k}^2 T_{n,m,k} + \sigma_{n,m,k}^2 (D_{n,m,k} + T_{n,m,k-1})}{\sigma_{n,m,k}^2 + \delta_{n,m,k}^2}. \quad (8)$$

The underground temperature and salinity fields resulting from application of the MLDE technique (Equation 8) are compared to results from application of the SLMVE technique in Figure 13. The transect position through the center of the Yellow Sea and the month (January) used Figure 13 is the same as in Figures 8 and 9, and the temperature and salinity above the bottom depth is the same as in the vertical-gradient-corrected GDEM4 transects (Figures 8b and 9b). The SLMVE technique applied to temperature and salinity (Figures 13 a and b, respectively) converted horizontal gradients (of temperature and salinity) along the sloping bottom bathymetry into vertical gradients underground. While we cannot know what the fields should look like underground, the strong underground gradients, particularly north of 34° N are clearly contrary to our expectations. We expect the vertical gradient immediately above the bottom to be continued downward below the bottom, change slowly with increasing depth below the bottom depth, and then blend gently into the surroundings. The single-level filling results are the antithesis of this expectation. The multi-level-dependent filling are comparable to what a person might have drawn by hand starting from the above-ground contours. Spot checks of the MLDE results in different seasons and various depths and conditions around the world, failed to reveal any obvious cases of faulty extrapolation.

7 Comparisons between GDEM4 and GDEM3 gridded fields

Global maps of the differences between the GDEM4 and GDEM3 temperatures and salinities and their standard deviations at several standard depths and months were prepared as a means of detecting errors in either of the climatologies. At positions where large differences were discovered, further examination of the two climatologies was made and, when required, comparisons to other climatologies such as the WOA2001Q2, WGHC, and to statistics computed from several years of satellite MCSST observations were also made. In this section, the discussion is limited to a small subset of the comparisons investigated in order to convey the most important findings.

7.1 Temperature and salinity differences

Figures 14 and 15 show temperature and salinity differences at 200 m depth (GDEM4 – GDEM3) in January and in August, respectively. Figures 16 and 17 show differences at 500 m depth, also for January and August, and Figure 18 shows difference at 1200 m. Figure 18 was prepared from the January climatology fields, but values at this depth represent an annual average since observations spanning all times of the year at this depth were used in its construction (see Table 1). In each figure, the range of values which determines the color of each difference was restricted to a subset of the total range in order to emphasize the primary regional differences. In addition, the absolute value of the differences is displayed in order to further reduce to the total range. A few of the strong differences outside these restricted ranges will also be discussed.

The salinity differences at 200 m in January, shown in Figure 14 a, identify several sites where differences are greater than 0.35 psu. The largest differences, over 1 psu, occur in the northeastern Red Sea. Maps of salinity, shown in Figure 19, at 200 m and 400 m in January from both the GDEM4 and GDEM3 climatologies reveal three low salinity patches along the coast of Saudi Arabia in GDEM3 that don't occur in GDEM4, WOA2001Q2, nor in WGHC (not shown). The west-to-east vertical section of salinity along 25° N across the full depth of the Red Sea (Figure 20) shows a full-depth east-west salinity gradient in GDEM3 that is not seen in GDEM4. In addition, the GDEM3 temperature also exhibits a full-depth temperature east-to-west change (not shown), about 1° C lower on the eastern side, that is not seen in GDEM4, WOA2001Q2, nor in WGHC. There is one small (probably erroneous) low-salinity patch in the GDEM4 climatology, approximately 0.05 psu lower than the surrounding salinity, near 23° N and 38° E (Figure 19), but it is minor compared to the errors in GDEM3.

Another large salinity difference at 200 m occurs in the southern Indian Ocean near 38° S and 86° E. As shown in Figure 21, the cause is apparently due to a line of erroneous salinity profiles with anomalously low salinities along 86° E from about 44° S to 26° S that were incorporated into the GDEM3 climatology. The resulting salinity error spans the depth range from the surface to at least 800 m, with largest errors at about 100 m, as shown in Figure 21 d.

The isolated salinity difference of about 0.35 psu centered near 150 E and 16 N at 200 m in January in Figure 14 a occurs in the North Equatorial Current, within the subsurface salinity maximum. Maps of salinity in this region, drawn from the GDEM4 and GDEM3 climatologies at 200 m are shown in Figure 22 together with west-to-east vertical sections down to 800 m depth through the region of the salinity difference. The GDEM4 salinity map (Figure 22 a) and vertical section (Figure 22 c) display the expected appearance of the salinity maximum, but the GDEM3 plots reveal a anomalous, and certainly erroneous, high-salinity region with about a 600 km diameter centered at about 150 m depth, extending from near the surface to about 500 m.

The next anomaly is centered near 142° W and 17° N and extends over a large area east of Mexico in the vicinity of the convergence of the North Equatorial current and the

Subtropical Gyre. The area encompassing this anomaly is expanded in Figure 23 which shows the salinity difference GDEM4-GDEM3 (not the absolute value as in Figures 14 through 18) on a map at 200 m depth and a south-to-north vertical section along 142° W. The larger negative anomaly (GDEM4 salinity lower than the GDEM3 salinity) extends from the surface to 250 m, spreading northward as it sinks. The maps and vertical sections of the salinities from the two climatologies shown in Figure 24 indicate that there is no obvious error in either climatology. Instead, the differences are amplified by small changes in the positions of the strong salinity fronts. In this case, there is no obvious error, and the difference can be attributed to differences in the data sets and differences in the interpolation parameters used in their construction. A similar conclusion appears to hold for the salinity anomaly off the east coast of South America seaward of the border between Uruguay and Argentina near 36° S approximately where the Malvinas Current and the Brazil Current meet (Figures 14, 15, and 16). An examination of the individual salinities from the two climatologies reveals no obvious errors, so the difference appears to be due to changes in the two data sets, probably attributable to the addition of new observations used in GDEM4 from Argos floats.

The temperatures of the two versions of GDEM generally show fewer regions of large differences than the salinity differences. In each case examined, no obvious fault from GDEM4 was found. Four of these regions will be discussed here. The first is centered near 169° E and 5° S at 200 m depth in January where the difference is about 2.5° C. Expanded maps of the GDEM4 and GDEM3 temperature at 200 m in this region and south-to-north vertical sections of temperature in the upper 500 m are shown in Figure 25. The maps of temperature from both climatologies are noisy with isolated highs and lows on the south side of the westward-flowing South Equatorial Current at about the latitude and longitude where the South Equatorial Counter Current starts. With no obvious error in either climatology, the differences appear to be a result of the large variability at this position and to differences in the data sets used in the construction of the two climatologies.

The next large temperature difference is seen at 104° E and 16° S in February at 200 m. The difference is also seen, but with smaller magnitude in the January global map of Figure 14 b. Expanded maps of temperature at 200 m and vertical south-to-north vertical sections of the upper 500 m from the two GDEM climatologies are shown in Figure 26. The cause of the large difference is an anomalously low temperature in the GDEM3 climatology extending from about 100 m to at least 400 m.

The next example of a temperature error comes from November in the region of the Atlantic North Equatorial Current. Figure 27 shows the temperature at 200 m depth and the west-to-east vertical section of temperature in the upper 500 m. The large difference between the two climatologies is due to an erroneous warm anomaly in the GDEM3 climatology from about 50 m depth to at least 350 m depth along a curved path starting at about 15° N and ending near 6° N.

The last temperature difference discussed here is the broad area from the Polar Front of the Southern Ocean to the Antarctic Continent inside the Continental Water boundary in

August (during Austral or southern Winter) south of the Indian Ocean. Along the Antarctic coastline temperature differences greater than 2.5° C extend from about 20° E to 160° E as shown in the temperature difference map at 200 m in August (Figure 15 b). As shown in the plots of the number of temperature profiles available in each ¼° x ¼° grid cell for gridding in the August GDEM4 climatology (Figure 28), the area south of 60° S is devoid of observations from the surface down to at least 800 m depth. At greater depths, the number observations increases due to the wider time-span used (all times of the year below 1200 m) as defined in Table 1. The lack of profiles during the Austral winter is due to the ice cover in much of the area south of 60° S. We have no information on the water temperature in the upper 800 m. The strategy in GDEM4 and in GDEM3 is to fill in the data-devoid regions by extrapolating from regions with data. GDEM4 starts with a first guess equal to the average in 1 latitude bands circling the globe. Then the interpolation equation (Eq. 2 with zero-gradient boundary conditions) is solved iteratively for a specified number of iterations (presently 3000 iterations). At the greatest distances from observations, convergence to a final steady state solution might never be reached, particularly in areas nearest the South Pole where meridians are closest together. Without convergence, the solution is somewhere between the initial values (the latitude band average) and the extrapolated data values. Small differences in methods used by GDEM4 and GDEM3, including the number of iterations and the time-span of observations used at each depth, can easily result in the temperature differences observed. Figure 29 shows regional maps of the GDEM4 and GDEM3 temperature near the Antarctic coast at 200 m. GDEM4 is missing the cold (less than 1° C) coastal water mass seen in GDEM3. Figures 29 c, d, and e show south-to-north vertical sections of temperature down to 800 m from the coast to 48° S from GDEM4, GDEM3, and the WOA2001Q2 climatologies, respectively. Compared to GDEM3 and WOA2001Q2, GDEM4 is missing the coldest water next to the coast between about 150m to 700 m depth. A possible means of fabricating a result that is more similar to the other climatologies is to rapidly expand the time span of the data used in constructing the August GDEM4 climatology below 150 m depth in this area. However, this modification is not presently planned.

7.2 Temperature and salinity standard deviation comparisons.

In this section, we start by comparing side-by-side global plots, shown in Figure 30 of the GDEM4 and GDEM3 temperature standard deviations at the surface at bi-monthly intervals. The range of standard deviations is limited to between 0° C and 2° C in order to display the same range as a function of color on each plot and to improve the display of the primary range of standard deviations. Three main differences between the standard deviations between the two versions of GDEM are readily apparent. First, the standard deviations in GDEM3 are much larger, by a factor of 1.5 to 2, than those of GDEM4. Further information is introduced later in this section to help determine correct magnitudes. The second primary difference is in the number and severity of localized large standard deviations (bull's-eyes). Small areas of large standard deviation are often caused by a few erroneous profiles with large anomalies from the local mean except

when they occur in areas where large variability is expected, such as near strong fronts. Bull's-eyes are prevalent in GDEM3 and rare in GDEM4. A third difference in GDEM3 is the discontinuity at 20° E, south of Africa, in the July and September. The global GDEM3 monthly climatologies, including the standard deviations, were constructed by splicing together four separate overlapping grids, each computed separately. The lines along the splices are not discernable in the resulting temperature and salinity grids, but are sometimes seen in the standard deviation grids, particularly for salinity standard deviation. GDEM4 was constructed by splicing together only two parts, the Arctic and everything else. The splicing lines were carefully chosen to eliminate discontinuities.

Although GDEM4 has much fewer obvious standard deviation errors than GDEM3, the accuracy of the estimates is still not known. More accurate estimates require a data set with a high density of observation at every location of the world's oceans. A product that approaches this goal is the MODAS2D monthly sea surface temperature climatology constructed from 15 years of MCSST observations. The MODAS2D standard deviations provide an excellent estimate of the truth to evaluate GDEM4, but it is only available at the surface and only for temperature. To infer the accuracy of the subsurface GDEM4 standard deviations requires that we assume that a good agreement between GDEM4 and MODAS2D at the surface suggests that GDEM4 standard deviations in the upper ocean might have a similar accuracy.

The surface temperature standard deviations from the WOA2005 and the MODAS2D monthly climatologies are shown on global maps at bi-monthly intervals in Figure 31. The WOA2005 standard deviations were computed for each month on a 1° x 1° global grid using only in situ observations from that month within each grid cell (centered on whole degrees of latitude and longitude). The grid cell is left blank when the number of observations is too few to make a reliable estimate. In both WOA2005 and MODAS2D the standard deviations for a particular month were computed using differences between the average for that month and all observations (for WOA2005) for all daily analyses (for MODAS2D) available in that month from all years. In GDEM4, the anomalies were computed as the difference between the observation and the set of monthly averages linearly interpolated to the position and time of year of the observation. The true variability about the moving mean should be computed as in GDEM4 because the random variability should be separated from the changes represented by mean seasonal cycle. As a result, the linear trend of the temperature change between each monthly average is added into the standard deviations of WOA2005 and the MODAS2D, but not into GDEM4. Therefore, the standard deviations of WOA2005 and MODAS2D are expected to be somewhat larger than those of GDEM4, particularly during Spring and Fall when the change between monthly averages is usually largest. A simple analysis shows that if the multi-year average of temperature changes linearly by X degrees C over a one month period (for all years) and the temperature anomalies from that linear trend have a constant standard deviation of Y degrees C during that month, then the standard deviation computed from anomalies about the mean of that month (as in WOA2005 and MODAS2D) is equal to $(Y^2 + X^2/12)^{1/2}$. The standard deviation computed in the same manner as GDEM4 in this case is equal to Y. For example, in the subtropical gyres of the North Atlantic and North Pacific, differences between monthly averages of consecutive

months can be as high as 3° C to 4° C, and the standard deviation in these areas with the linear trend removed may be only about 1° C. The combined standard deviation is then $(1^2+3.5^2/12)^{1/2} = 1.42^\circ \text{ C}$ and the combined standard deviation is 2.24° C if the background standard deviation is 2° C.

In Figure 31, the WOA2005 and MODAS2D often match well in areas where in situ data is plentiful. There is often large variability in magnitude within any local group of pixels in the WOA2005 maps, and visually eliminating the pixels with the smaller magnitudes results in the best match to the MODAS2D maps. If the WOA2005 maps were spatially smoothed to remove the small scale pixel-by-pixel variation, the resulting standard deviation maps would have magnitudes similar to those in GDEM4. Also, as explained previously, the standard deviations are often larger in WOA2005 and MODAS2D because they include variation from the seasonal trend. The surface GDEM3 temperature standard deviations north of 30° N are too large compared to MODAS2D, often filling the entire area up to the Arctic with values exceeding 2° C. The GDEM4 fields are typically weaker, more diffuse, and more variable than those of MODAS2D, but otherwise the overall agreement is good, particularly considering that MODAS2D includes variance from the seasonal changes and that GDEM4 doesn't.

The temperature standard deviations at 500 m depth are shown in Figure 32. Included in this figure are the standard deviations from GDEM4 in February (which uses data spanning 3 months at this depth), from GDEM3 in February, from the WOA2005 seasonal grid in winter, and from the annual WGHC. The larger number of in situ observations available over a full season results in fewer blank cells in WOA2005, and the added variance caused by including the seasonal trend is expected to be very small at this depth. The GDEM4 and WOA2005 maps agree well. The GDEM3 map is noisier than GDEM4 and includes several erroneous bull's-eyes. The annual standard deviation from WGHC is completely different from the other climatologies.

The temperature standard deviations at 1000 m depth from the same four climatologies as Figure 32 are shown in Figure 33. The time span of the observations at 1000 m in GDEM4 is annual so that the GDEM4 plot in Fig 30a is labeled as annual even though it was made from the February climatology. The WOA2005 plot is made from the annual climatology, and WGHC climatology is annual at all depths. The GDEM4 and WOA2005 standard deviations agree well, but GDEM4 magnitudes are smaller, particularly in the Gulf Stream and North Atlantic Current frontal regions. The GDEM3 standard deviations are noisier, but otherwise similar to those of GDEM4. Once again, the WGHC appears to be unrelated to the other climatologies.

Global maps comparing salinity standard deviations from GDEM4, GDEM3, WOA2005, and WGHC are shown at 500 m depth in Figure 34 and at 1000 m depth in Figure 35. The range of values are restricted to between 0 psu and 0.2 psu at 500 m and between 0 psu and 0.1 psu at 1000 m, although the maximum range in each of the maps exceeds the maximum limit at some positions. The GDEM4 and WOA2005 the salinity standard deviations at 500 m compare favorably in regions where the density of gaps in WOA2005 permit such comparisons. The magnitudes of the WOA2005 values are larger than those

in GDEM4 in some area, such as of the California coast and near Hawaii. The GDEM3 salinity standard deviation map (Figure 34 b) has many bull's-eyes scattered throughout it, whereas GDEM4 has none at this depth. In addition, the magnitudes of the standard deviations throughout many of the areas far from strong fronts is much higher (0.06 psu to 0.09 psu) than seen in GDEM4 or WOA2005 (0.01 to 0.04 psu). As with the temperature standard deviations, the WGHC salinity standard deviations are completely unlike those in the other climatologies.

The salinity standard deviations at 1000 m (Figure 35) in GDEM4 are similar to those in WOA2005 in the few regions where the WOA2005 map is not blank. The GDEM3 standard deviations at 1000 m are primarily made up of bull's-eyes and bear little resemblance to either GDEM4 or WOA2005 except off the coast of Portugal in the high variability region occupied by meddies. As in all other cases examined, the WGHC map is surprising, at best.

8 Conclusions

The methods used in the construction of the GDEM4 climatology described in this report are similar to those used in the construction of GDEM3, with only small changes to numerical methods and choices of parameters. Due to the increased memory size of the computers used with GDEM4, the entire global grid was computed in core (except for the Arctic) without the need to splice grids together to form a complete global grid as was done with GDEM3, eliminating small discontinuities at splice points. The vertical gradient correction employed in both GDEM3 and GDEM4 were shown to correct biases in the gridded fields caused by changes in the number and type of observations versus depth available for gridding. These corrections were shown to be particularly effective in shallow coastal regions with sloping bottom topography and where strong offshore gradients of the temperature or salinity are found.

The bottom depth topography grid used with GDEM4 was derived from a higher-resolution topography (NRL's DBDB2) than the topography used with GDEM3 (NAVO's DBDB5, although DBDB5 contributed to the construction of DBDB2). In addition, the deepest DBDB2 depth within the $\frac{1}{4}^\circ$ cell centered at each climatology grid point was used to form the bottom depths of GDEM4, whereas the GDEM3 depths were derived by bilinear interpolation from DBDB5. As a result, the GDEM4 depths are somewhat deeper than those of GDEM3, on the average.

The greatest improvement in GDEM4 as compared to GDEM3 is in the increased size and the improved quality of the profile data set used. A total of 4,412,454 temperature profiles and 1,969,081 salinity profiles were used in the construction of GDEM4, whereas only 1,732,013 temperature profiles and 998,225 salinity profiles were used with GDEM3. The improved quality of the editing of the GDEM4 data set is evident in the significantly reduced magnitudes and numbers of erroneous bull's eyes in the standard deviation plots from the GDEM4 climatology as compared to those of GDEM3.

Two new products have been added to the GDEM4 climatology. One is the set of monthly global grids for every month spanning all depths of the number of temperature and the number of salinity observations used in the construction of GDEM4. The other is the set of filled grids of temperature and salinity and their standard deviations. The filled grids extrapolate the values underground using a new technique developed for GDEM4 that is a significant improvement over methods previously employed.

Plots of global temperature difference and salinity differences between the GDEM4 and GDEM3 monthly mean climatologies were constructed at many depths and for several different months. Many of the plots revealed several small areas where the differences were exceptionally large. Further examination of the temperature and salinity fields from both climatologies in these areas confirmed that the large differences were due either to errors in the GDEM3 climatology, but not in GDEM4, or to differences in the numbers and types of profiles used in their construction, but apparently not to errors in either. In one case, along a portion of the Antarctic coastline, large differences were attributed to the lack of any data in the upper ocean within about 600 km of the coastline during August (Austral winter) due to ice cover. Without observations, the true nature of the temperature and salinity structure in this area is not known.

Global maps of temperature standard deviation in each month of the year were compared among GDEM4, GDEM3, WOA2005, and MODAS2D. The exceptionally large number of satellite MCSST observations available in the construction of the MODAS2D monthly sea surface temperature and temperature standard deviation climatology make it the best estimate of the truth among the climatologies. The GDEM4 standard deviations are typically smaller and more diffuse than those of MODAS2D, but the agreement between the two is generally good. The GDEM3 standard deviations are often too large and contain a large number of erroneous bull's-eyes. The GDEM4 and WOA2005 monthly surface temperature standard deviations agree well, though the large pixel-to-pixel variability and the large number of voids (where sufficient data were unavailable to provide an estimate) in the WOA2005 fields make comparisons difficult.

Temperature and salinity standard deviations at 500 m and 1000 m depth were compared among GDEM3, GDEM4, WOA2005, and WGHC. GDEM3 compared well with WOA2005 at both depths for both temperature and salinity standard deviations. GDEM3 temperature standard deviations at 500 m depth and salinity standard deviations at both the 500 m and 1000 m depths exhibited copious numbers of bull's-eyes. Comparisons to the WGHC standard deviations were not useful because those fields were completely unlike those of the other climatologies.

In all of the evaluations performed, the GDEM4 climatology has been shown to be a significant improvement over GDEM3. GDEM4 combines the methodology originally developed for GDEM3 with a significantly improved observation data set to form a high-quality high-resolution climatology which can be employed with confidence by the U.S. Navy.

9 References

Antonov, J. I., R. A. Locarnini, T. P. Boyer, A. V. Mishonov, and H. E. Garcia, 2006, World Ocean Atlas 2005, Volume 2: Salinity. S. Levitus, Ed. NOAA Atlas NESDIS 62, U.S. Government Printing Office, Washington, D.C., 182 pp.

Arctic Climatology Project, 1997, *Environmental Working Group joint U.S.-Russian atlas of the Arctic Ocean - winter period*. Edited by L. Timokhov and F. Tanis. Ann Arbor, MI: Environmental Research Institute of Michigan in association with the National Snow and Ice Data Center. CD-ROM.

Arctic Climatology Project, 1998, *Environmental Working Group joint U.S.-Russian atlas of the Arctic Ocean - summer period*. Edited by L. Timokhov and F. Tanis. Ann Arbor, MI: Environmental Research Institute of Michigan in association with the National Snow and Ice Data Center. CD-ROM.

Bauer, R., 1982, Functional Description: Master Oceanographic Data Set (MOODS), Compass Systems Inc.

Boyer TP, Stephens C, Antonov JI, Conkright ME, Locarnini RA, O'Brien TD, Garcia HE, 2002, World Ocean Atlas 2001 *Volume 2: Salinity*, Levitus S (ed). *NOAA Atlas NESDIS 50*. US Government Printing Office: Washington, DC.

Boyer. T.P., J.I. Antonov, H.E. Garcia, D.R. Johnson, R.A. Locarnini, A.V. Mishonov, M.T. Pitcher, O.K. Baranova, I.V. Smolyar, 2006, World Ocean Database 2005. S. Levitus, Ed., NOAA Atlas NESDIS 60, U.S. Government Printing Office, Washington, D.C., 190 pp., DVDs.

Boyer, T., P. Levitus, H. Garcia, R. Locarnini, C. Stephens, and J. Antonov, 2005, Objective analysis of annual, seasonal, and monthly temperature and salinity for the World Ocean on a 0.25 grid, *Int. J. of Clim.*, 25, 931-945.

Brasseur, P., J.M. Beckers, J.J. Brankart, and R. Schoenauen, 1996, Seasonal temperature and salinity fields in the Mediterranean Sea: Climatological analyses of an historical data set. *Deep-Sea Res.*, 43, 159-192.

Briggs, I.C., 1974, Machine contouring using minimum curvature, *Geophysics*, 39, 39-48.

Carnes, M.R., 2009, Description and Evaluation of GDEM-V 3.0, NRL Memorandum 7330—09-9165, 21 pp.

Gouretski, V.V. and K.P. Koltermann, 2004, WOCE Global Hydrographic Climatology. 35/2004, Berichte des Bundesamtes für Seeschifffahrt und Hydrographie, 52 pp.

Jackett, D.R. and T.J. McDougall, 1995, Minimal adjustment of hydrographic profiles to achieve static stability, *J. Atmos. and Ocean. Tech.*, 12, 381-389.

Jugan, M.J., and H. Beresford, 1991, Editing Approach for the Navy's Master Oceanographic Observation Data Set, Published in Proceedings of MTS '91, An Ocean Cooperative: Industry, Government, and Academia, Vol. II.

Kara, A.B., C.N. Barron, and T.P. Boyer, 2009, Evaluations of SST climatologies in the tropical Pacific Ocean, *J. Geophys. Res.*, 114, C02021, doi:10.1029/2008JC004909

Ko, D.S, 2009. DBDB2 v3.0 Global 2-Minute Topography, http://www7320.nrlssc.navy.mil/DBDB3_WWW. Naval Research Laboratory, Oceanography Division, Ocean Dynamics and Prediction Branch.

Locarnini, R. A., A. V. Mishonov, J. I. Antonov, T. P. Boyer, and H. E. Garcia, 2006, World Ocean Atlas 2005, Volume 1: Temperature. S. Levitus, Ed. NOAA Atlas NESDIS 61, U.S. Government Printing Office, Washington, D.C., 182 pp.

Lozier, S. M., M. S. McCartney, and W. B. Owens, 1994, Anomalous anomalies in averaged hydrographic data. *J. Phys. Oceanogr.*, 24, 2624-2638.

Marks, K.M. and W.H.F. Smith, 2006, An evaluation of publicly available bathymetry grids, *Mar. Geophys. Researches*, 27, 19-34.

Panteleyev, G. G. and M.I. Yaremchuk, 1989, A procedure for interpolating current speed observations at automated buoy stations, *Oceanology*, 29, 298-301.

Panteleev, G. G. and Yu.B. Filyushkin, 1995, A comparative analysis of the methods of optimal and variational interpolation of data on the velocity of oceanic currents, *Oceanology*, 35, 16-19.

Shapiro, R, Smoothing, filtering, and boundary effects, 1970, *Rev. Geophys. Space Physics*. 8, 359-387.

Smith, W. H. and P. Wessel, 1990, Gridding with continuous curvature splines in tension, *Geophysics*, 55, 293-305.

Smith, W. H. F., and D. T. Sandwell, 1997, Global seafloor topography from satellite altimetry and ship depth soundings, *Science*, v. 277, p.1957-1962, 26 Sept.

Steele, M., R. Morley, and W. Ermold, 2001, PHC: A global ocean hydrography with a high quality Arctic Ocean, *J. Climate*, 14, 2079-2087.

Stephens C, Antonov JI, Boyer TP, Conkright ME, Locarnini RA, O'Brien TD, Garcia HE, 2002, *World Ocean Atlas 2001 Volume 1: Temperature*, Levitus S (ed.). NOAA Atlas NESDIS 49. US Government Printing Office: Washington, DC.

Swain, C.J., 1976, A FORTRAN IV program for interpolating irregularly spaced data using the difference equations for minimum curvature, *Computers & Geosciences*, 1, 231-240.

Teague, W.J., M.J. Carron, and P.J. Hogan, 1990, A comparison between the Generalized Digital Environmental Model and Levitus climatologies. *J. Geophys. Res.*, 95 (C5), 7167-7183.

10 Tables

Table 1 Number of profiles of each instrument type before and after each step in removal. The "Instrument Type Number" refers to the description of each type of instrument in Table 2. "Original Number" is the number of temperature profiles (with or without corresponding salinity profiles) of raw unedited data. The third column, "Number Removed", is the number of profiles removed either because they removed during manual quality control, because the number of observation depths is less than 2, or the instrument type was 2, 69 or 70 (MBT, moored buoy, drifting buoy), and the fourth column list the number of temperature profiles remaining after the removal. The fifth column list the number of profiles removed because the bottom bathymetry depth was greater than or equal to 400 m, but the greatest depth of the profiles was less than 200 m. The sixth and seventh columns list the final number of temperature and salinity profiles, respectively, remaining in the final profile data used in the construction of GDEM4. The totals from columns two through seven are listed in the bottom row.

Instrument Type Num.	Original Number	Number Removed	Number Remaining	Number Removed	Final Temperature	Final Salinity
1	682052	-52513	629539	-85212	544327	38623
2	2237379	-2237379	0	0	0	0
4	3130	-4	3126	0	3126	3126
5	83	-9	74	0	74	74
9	150	0	150	-3	147	0
10	3749	-228	3521	-197	3324	0
11	1981268	-204678	1776590	-95244	1681346	1
12	56487	-2777	53710	-932	52778	0
13	105	-18	87	-3	84	0
15	1	0	1	-1	0	0
18	4018	-5	4013	0	4013	0
19	38	-1	37	0	37	37
25	1708992	-437824	1271168	-41393	1229775	1173847
30	34128	-3056	31072	-2897	28175	28076
31	13274	-2122	11152	-183	10969	10254
32	656	-181	475	-4	471	469
33	494042	-70821	423221	-12725	410496	403331
35	1289	-80	1209	-93	1116	1116
36	7737	-1348	6389	-207	6182	6182
37	1962	-1311	651	-3	648	592
38	5392	-377	5015	-50	4965	4965
41	7388	-139	7249	-41	7208	7208
42	128	-1	127	-1	126	126
43	1138	-108	1030	-17	1013	1013
51	290107	-55095	235012	-2012	233000	215169
62	9685	-1397	8288	-90	8198	6477
64	81940	-30468	51472	-478	50994	41695
65	8443	-79	8364	-623	7741	7741
68	27130	-22184	4946	-159	4787	0
69	384162	-384162	0	0	0	0
70	101252	-101252	0	0	0	0
71	21225	-1083	20142	-5448	14694	14573
73	133667	-10399	123268	-20628	102640	4386
Total	8302197	-3621099	4681098	-268644	4412454	1969081

Table 2 Description of the measurement instrument for each instrument type number listed in Table 1.

Instrument Type Number	Description of Instrument Type
1	Message data (regardless of instrument)
2	Mechanical Bathythermograph (MBT)
4	SEABIRD CTD Time Series
5	Air-deployed CTD (AXCTD)
9	Ship deployed AXBT
10	Some unknown electronic temperature depth instrument
11	Expendable bathythermograph
12	Air deployed expendable bathythermograph
13	Submarine deployed expendable bathythermograph (SXBT)
15	Expendable sound velocity profiler (XSV)
18	Time Series XBT (TSXBT)
19	Submarine deployed CTD
25	Hydrocast: bottles and reversing thermometers
30	Unknown electronic salinity, temp., depth instruments
31	Salinity, temperature and depth probe (STD)
32	Low-resolution STD from NODC
33	Conductivity, temperature, depth probe (CTD)
35	CTD time series (YO-YO)
36	Sound velocity, salinity, temp, and depth (SVSTD)
37	Sippican XCTD
38	Seabird CTD SBE-19 (Seacat profiler)
41	Seabird CTD SBE-911 (deep ocean)
42	Seabird CTD SBE-25
43	Falmouth CTD
51	Argo/Palace floats
62	tesac RTDHS message data
64	Palace/Apex floats RTDHS message data
65	Glider RTDHS message data
68	Autonomous Pinniped Buoy (APB)
69	Moored buoy (MRB)
70	Drifting buoy (DRB)
71	Undulating ocean recorder (UOR)
73	Unknown instrument

Table 3 Total two-sided time range in days versus depth range of profiles used in the construction of each GDEM4 monthly climatology

Depth Range (m)	Time Range (days)
0 - 200	45
220 - 400	60
500 - 800	90
900 - 1200	120
1300 - 6600	366

11 Figures

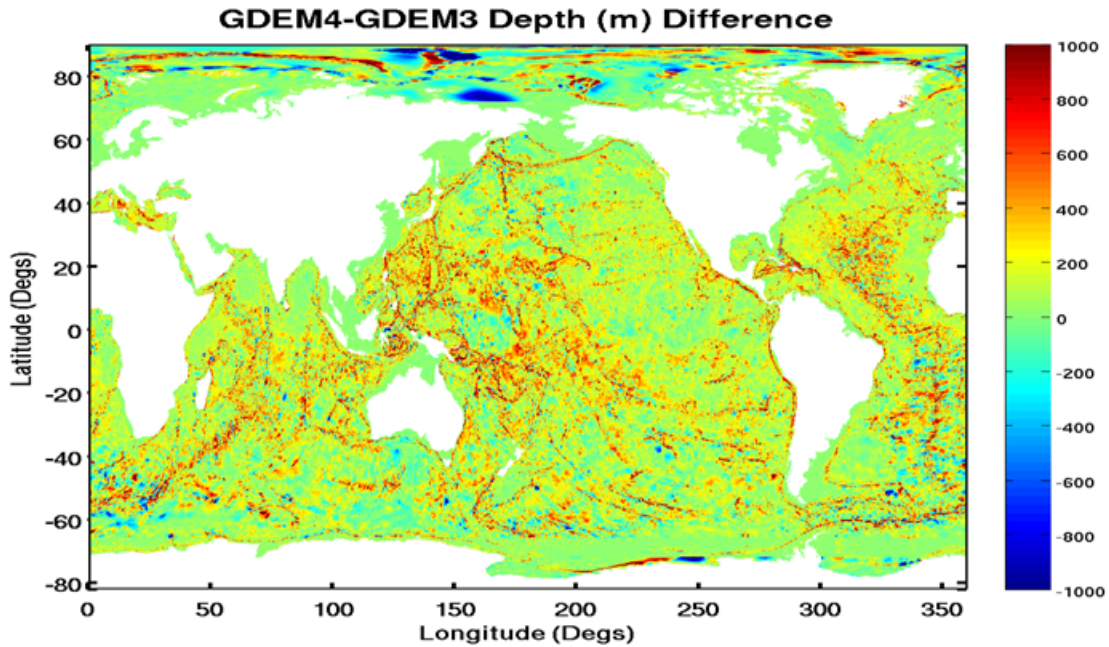


Figure 1 Global map of the bottom bathymetry depth difference (m) at each grid node of the GDEM4 and GDEM3 climatologies. Differences were computed as the GDEM4 depths minus the GDEM3 depths. The total range of the differences is over 4000 m, but the color range has been restricted to +/-1000 m to highlight the central range of differences.

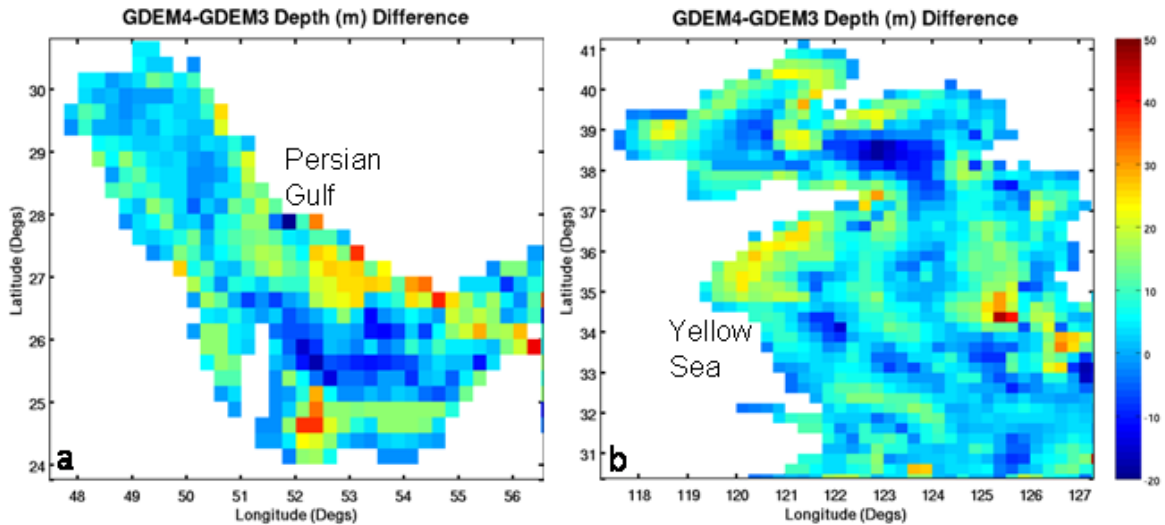


Figure 2 Maps of the bottom bathymetry depth differences (GDEM4 –GDEM3) in (a) the Persian Gulf and (b) the Yellow Sea. The pixel coloring is restricted to the range of -20 m to 50 m in both maps.

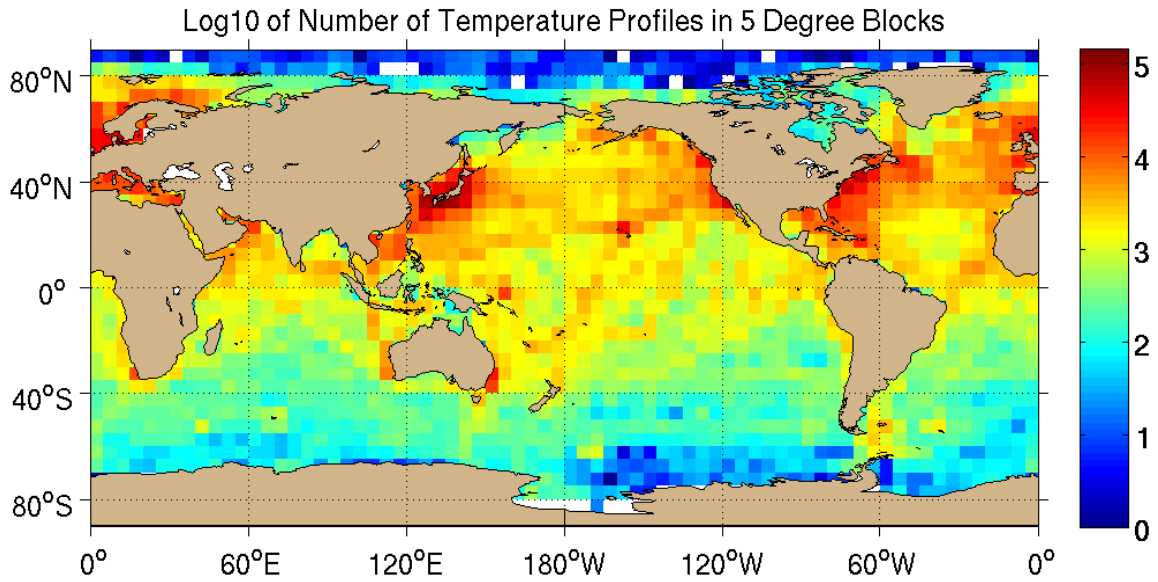


Figure 3 Log₁₀ of the number of temperature profiles used in the construction of the GDEM4 climatology within each 5° x 5° (latitude, longitude) cell. No profiles were available within grid cells colored white.

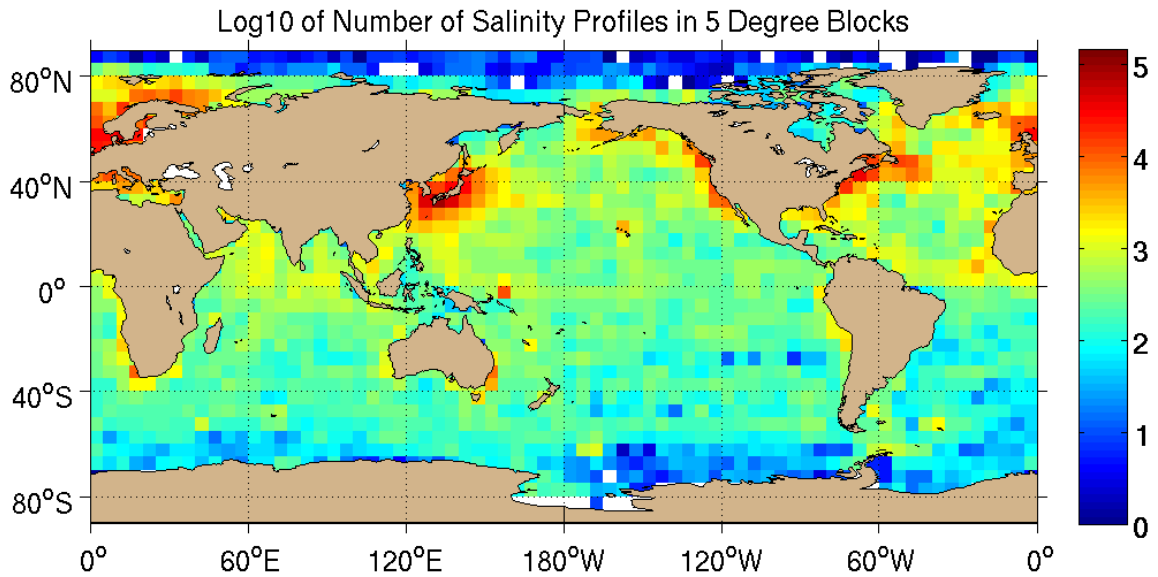


Figure 4 Log₁₀ of the number of salinity profiles used in the construction of the GDEM4 climatology within each 5° x 5° (latitude, longitude) cell. No profiles were available within grid cells colored white.

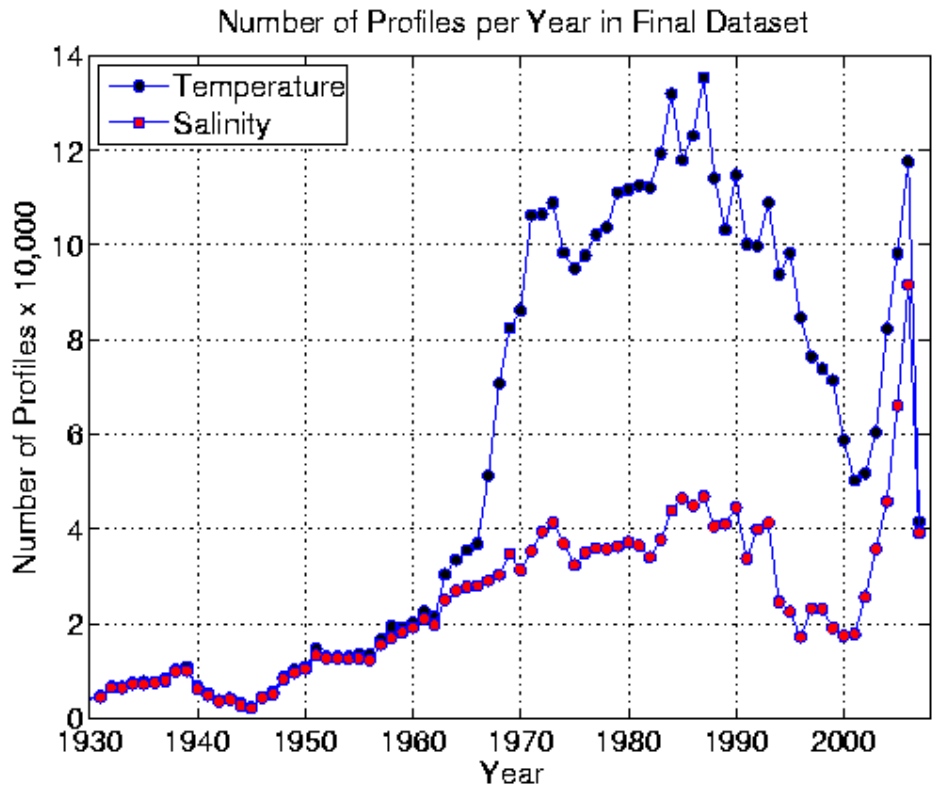


Figure 5 Number of profiles of temperature (blue-filled circles) and salinity (red-filled circles) used in the construction of GDEM4 measured in each year. The plot was restricted to years after 1930 for clarity, although the first date of observation in the data set was September 22, 1817. The last date of the observations is October 11, 2007.

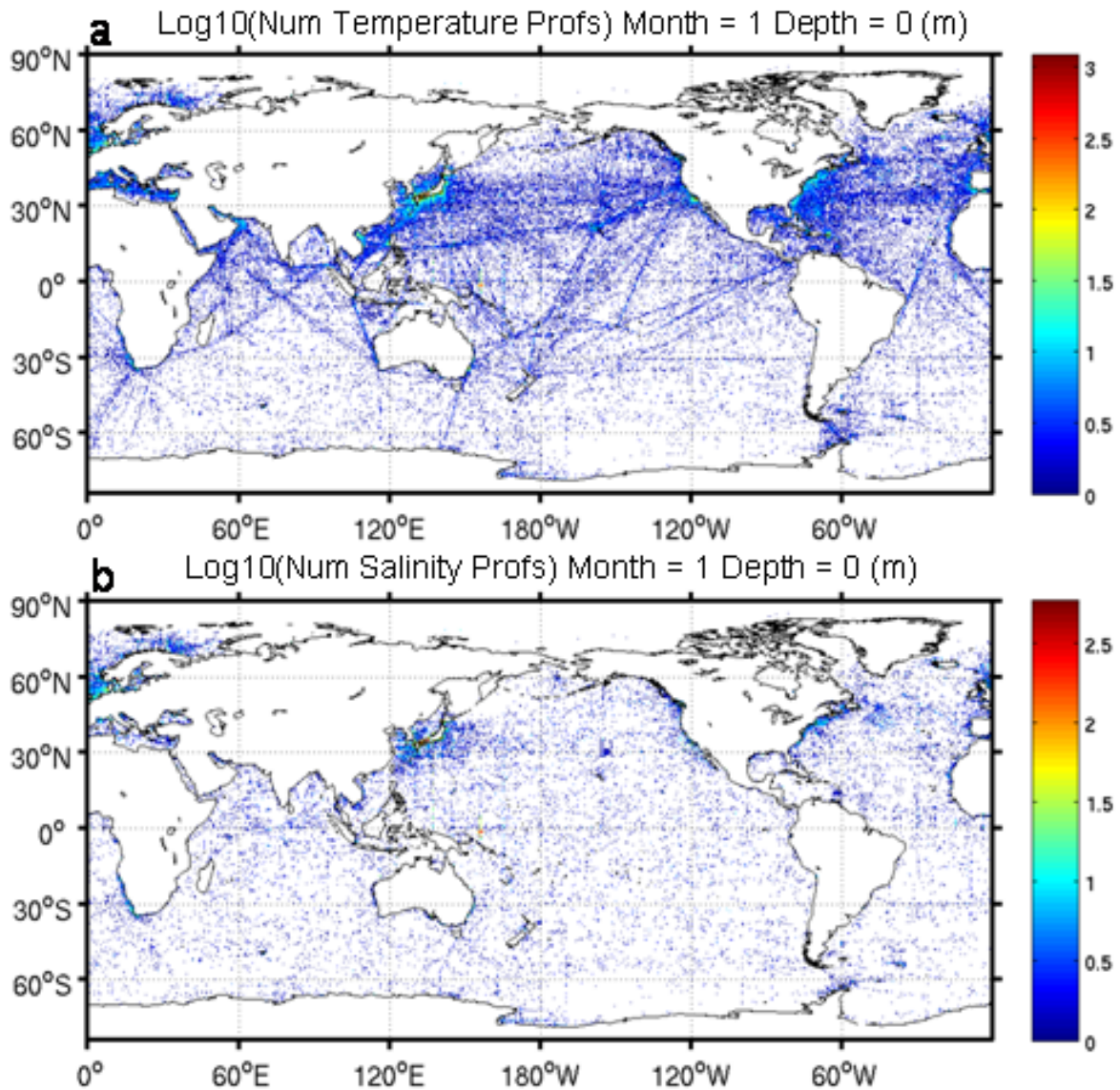


Figure 2 Global maps of the \log_{10} of the number of observations (of temperature or salinity, as specified) within each $1/4^\circ \times 1/4^\circ$ grid cell at the specified depth used to compute the January GDEM4 monthly mean and standard deviation climatologies. No observations were available within cells colored white.

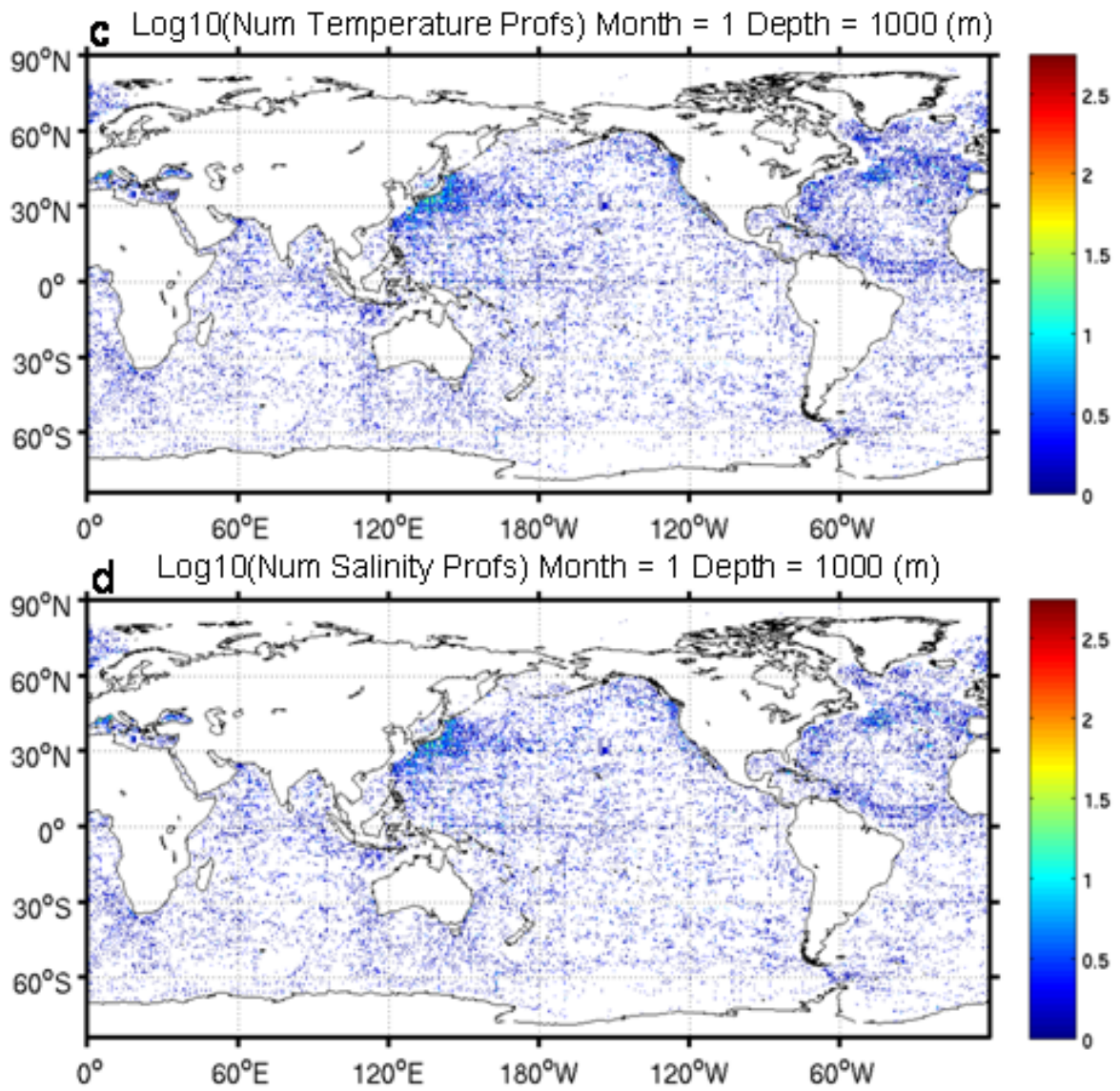


Figure 6 (continued).

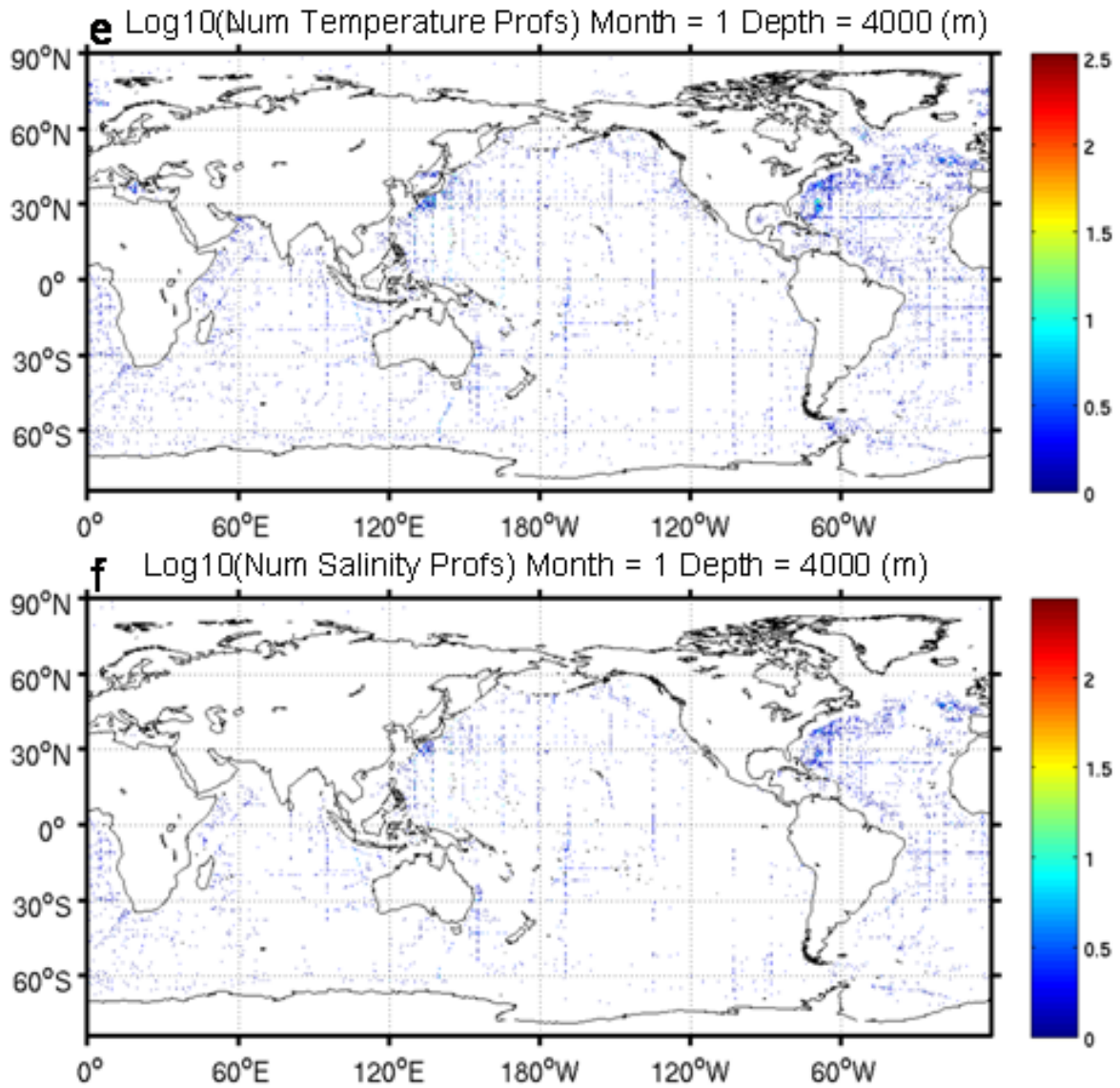


Figure 6 (continued).

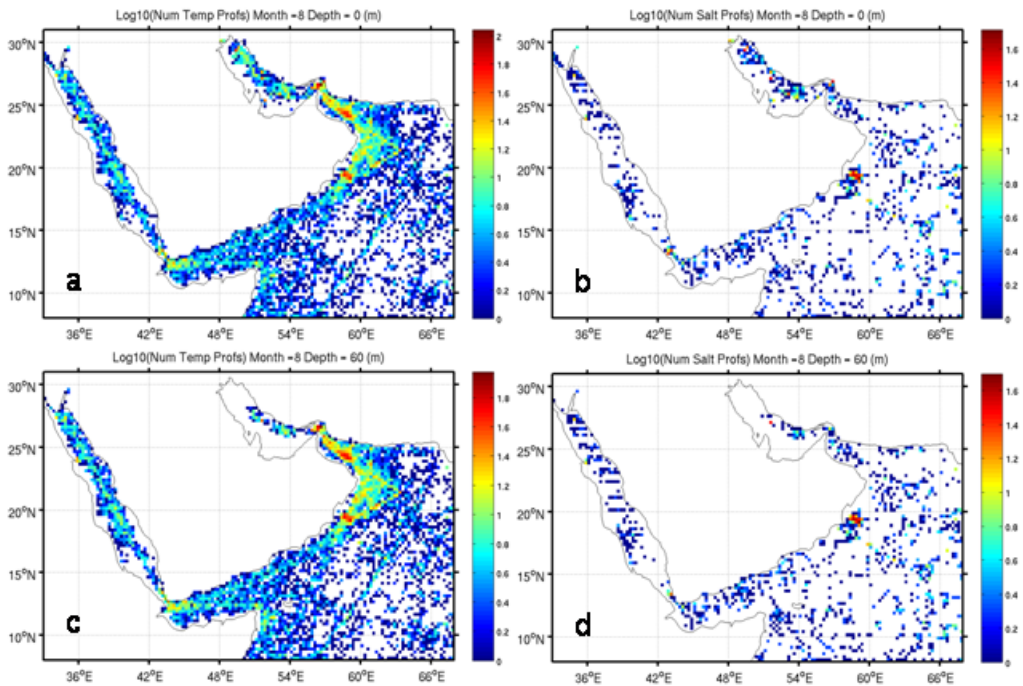


Figure 7 Maps in the area of the Red Sea, Gulf of Aden, Gulf of Oman, Arabian Gulf, and Arabian Sea of the log₁₀ of the number of observations of (a and c) temperature and (b and d) salinity within each $\frac{1}{4}^\circ \times \frac{1}{4}^\circ$ grid cell at (a and b) the surface and (c and d) at 60 m depth used to compute the August GDEM4 monthly mean and standard deviation climatologies. No observations were available within cells colored white.

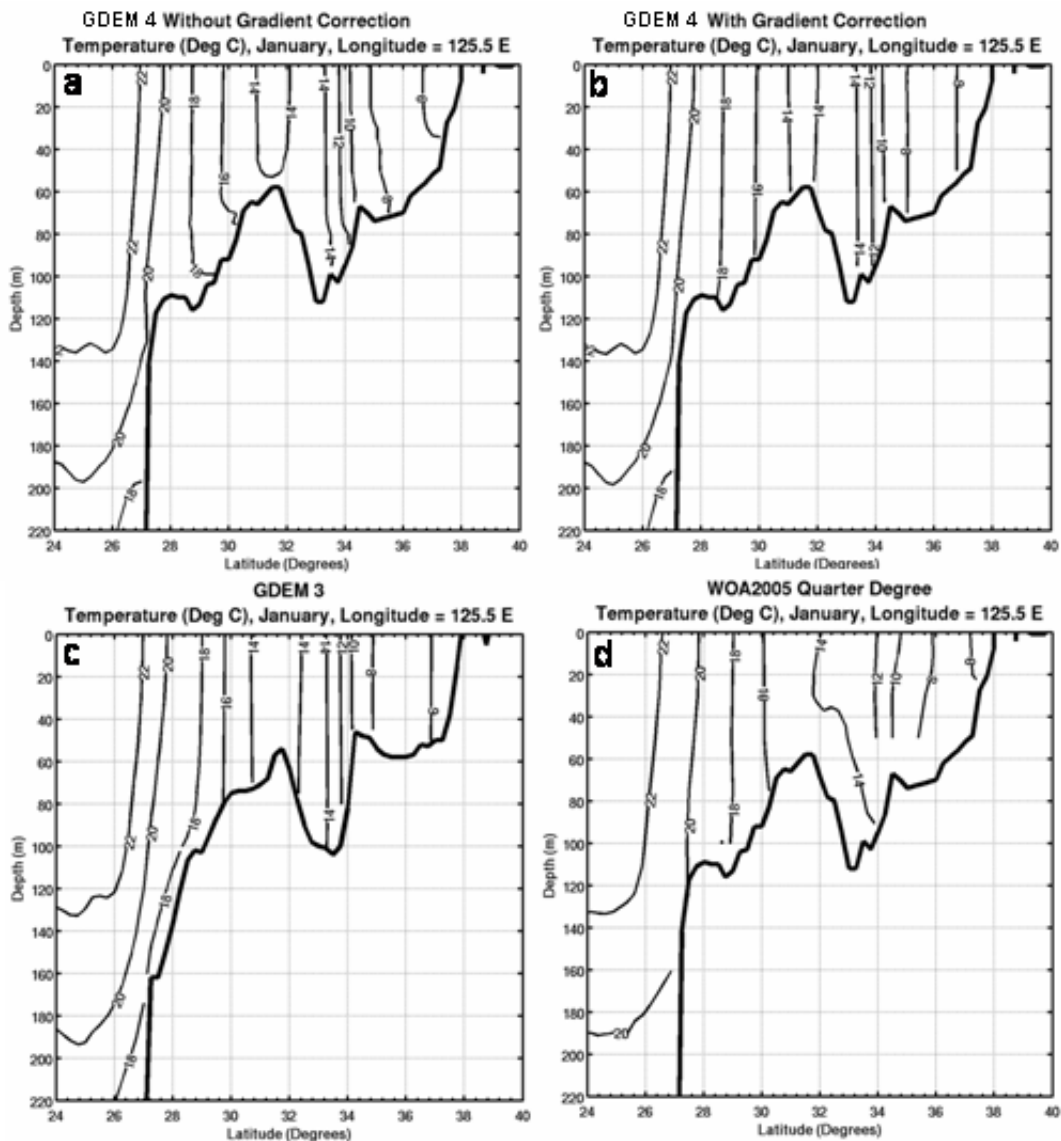


Figure 8 Contours of temperature in January along a south-to-north transect from the Okinawa trough to the north end of the Yellow Sea along 125.5° E. Temperatures are taken from GDEM4 (a) before and (b) after application of the vertical gradient correction, GDEM3 (which had a similar vertical gradient correction applied), and the 1/4°-resolution WOA. Both the uncorrected GDEM4 and the WOA contours shows temperature inversion (temperature increasing downward).

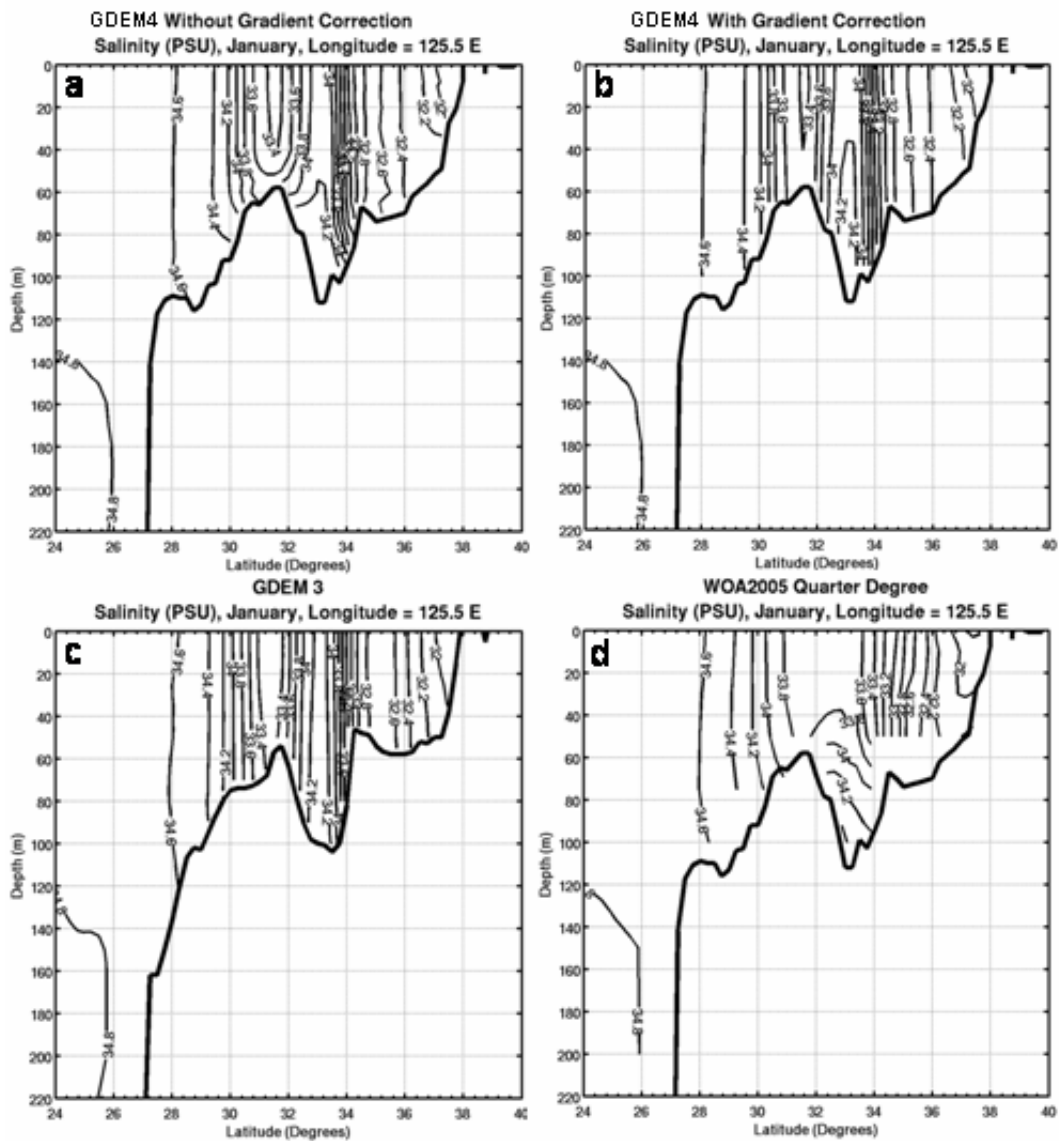


Figure 9 Contours of salinity in January along a south-to-north transect from the Okinawa trough to the north end of the Yellow Sea along 125.5° E. Salinities are taken from GDEM4 (a) before and (b) after application of the vertical gradient correction, (c) GDEM3 (which had a similar vertical gradient correction applied), and (d) the 1/4 -resolution WOA.

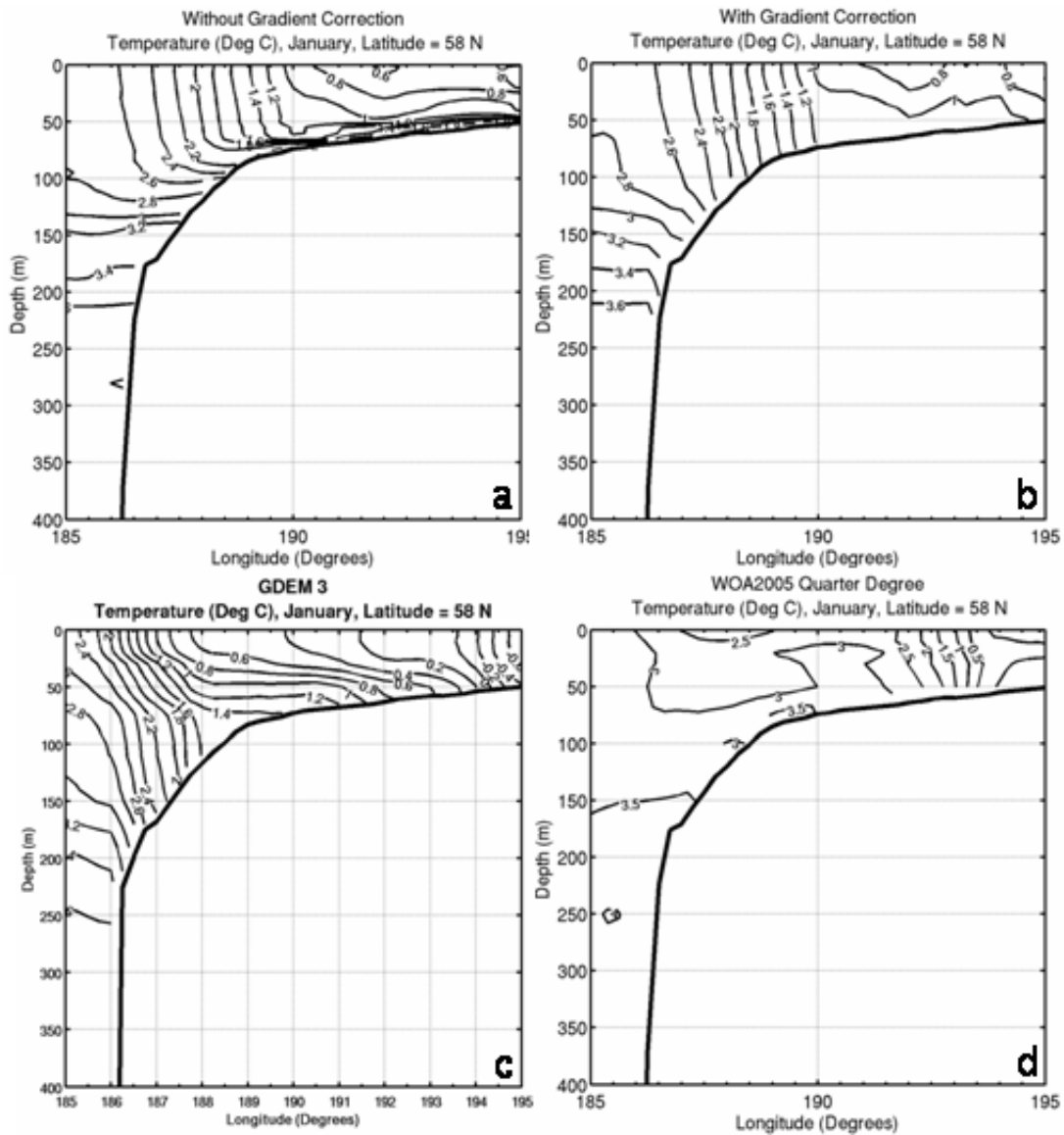


Figure 10 Contours of temperature in January along a west-to-east transect over the eastern Bering Sea shelf and slope east of Bristol Bay along 58° N. Temperatures are taken from GDEM4 (a) before and (b) after application of the vertical gradient correction, (c) GDEM3 (which had a similar vertical gradient correction applied), and (d) the 1/4 -resolution WOA.

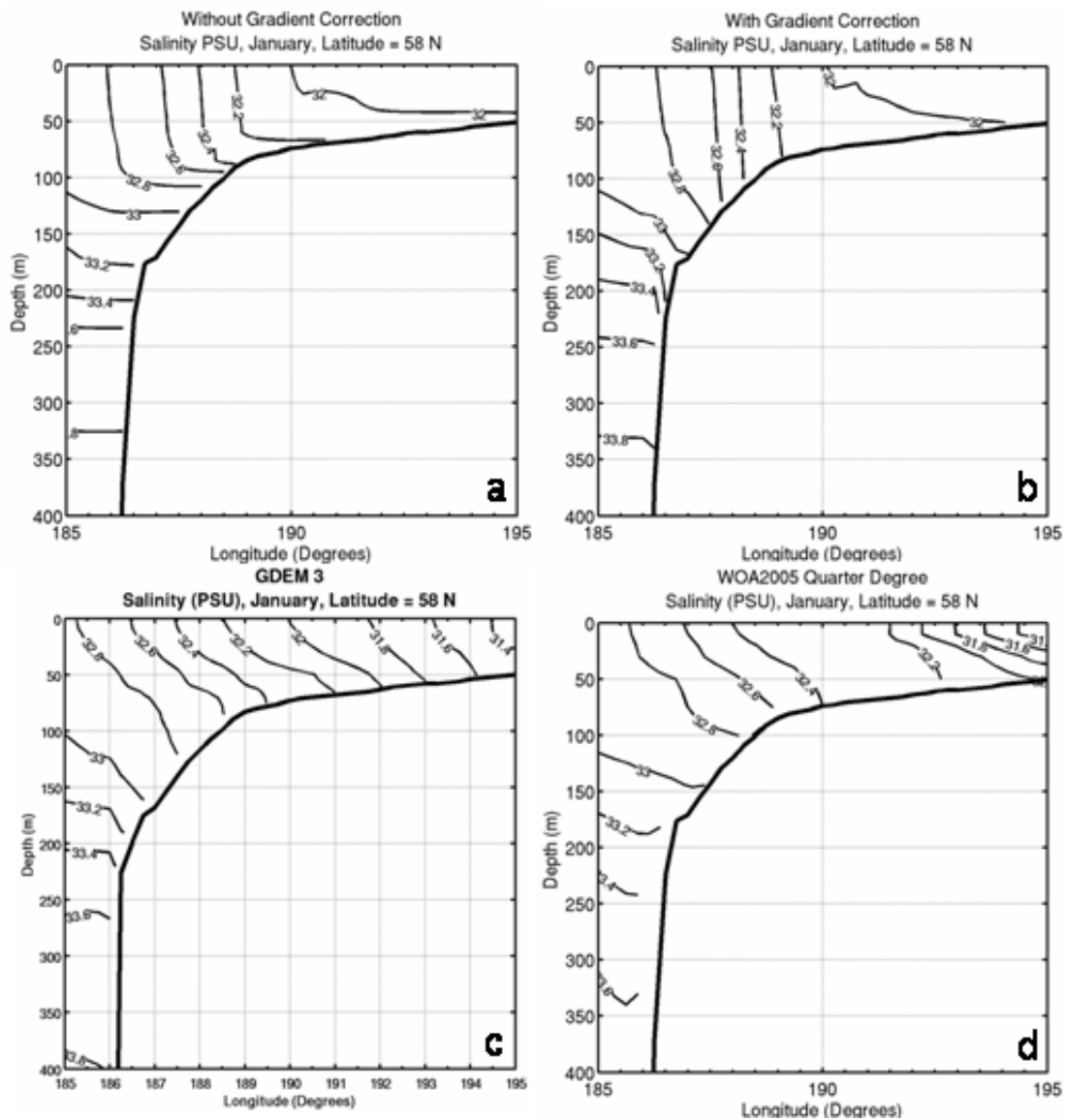


Figure 11 Contours of salinity in January along a west-to-east transect over the eastern Bering Sea shelf and slope east of Bristol Bay along 58° N. Salinities are taken from GDEM4 (a) before and (b) after application of the vertical gradient correction, (c) GDEM3 (which had a similar vertical gradient correction applied), and (d) the ¼ -resolution WOA.

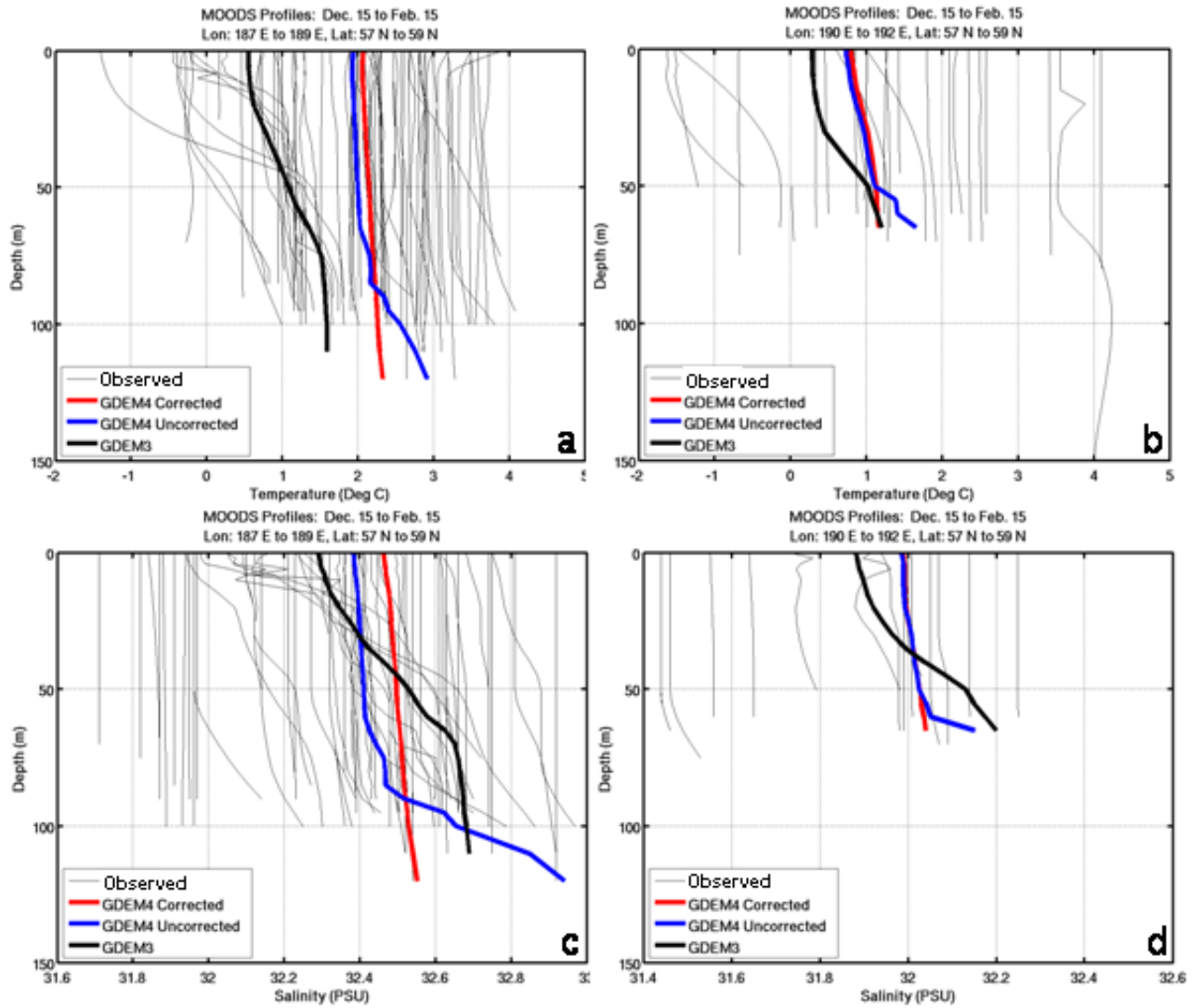


Figure 12 Profiles of (a, b) temperature and (c, d) salinity in January at and surrounding two locations along the eastern Bering Sea transect shown in Figures 7 and 8. Profiles from the GDEM4 climatology prior to correction by the vertical gradient correction (thick blue line), the GDEM4 climatology after correction (thick red line), and the GDEM3 climatology (thick black line) are located at 58° N and 188° E over the shelf break in frames a and c at 58° N and 191° E in frames b and d. The thin grey lines are profiles from the archive used in the construction of GDEM4 within 1 degree of latitude and longitude from the locations of the climatology profiles (thick lines).

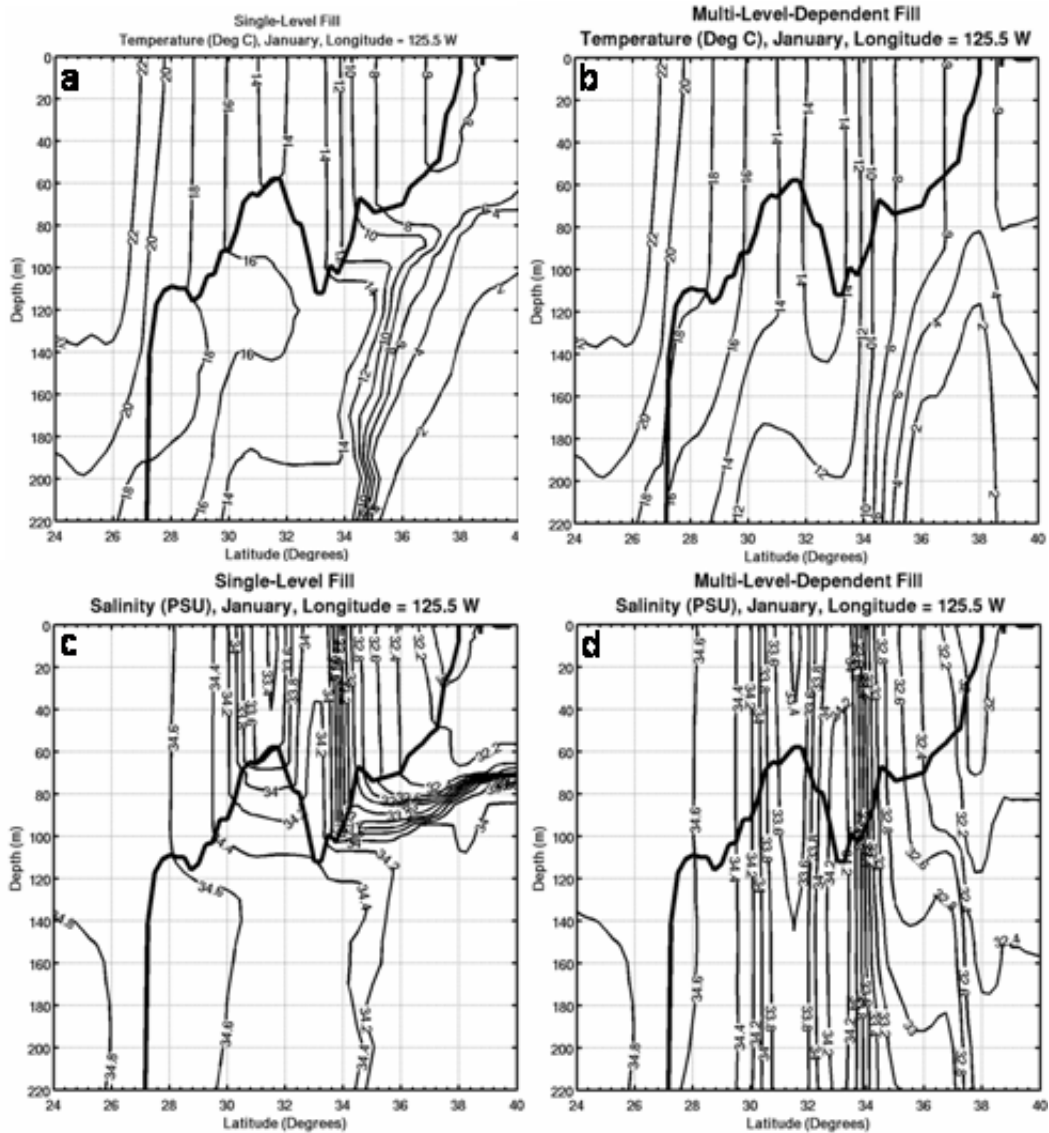


Figure 13 Contours of GDEM4 January (a, b) temperature and (c, d) salinity along a south-to-north transect from the Okinawa trough to the northern end of the Yellow Sea along 125.5° E. The underground domain was filled by the single-layer median-value extrapolation (SLMVE) technique in frames a and c, and by the multi-level-dependent extrapolation (MLDE) technique in frames b and d.

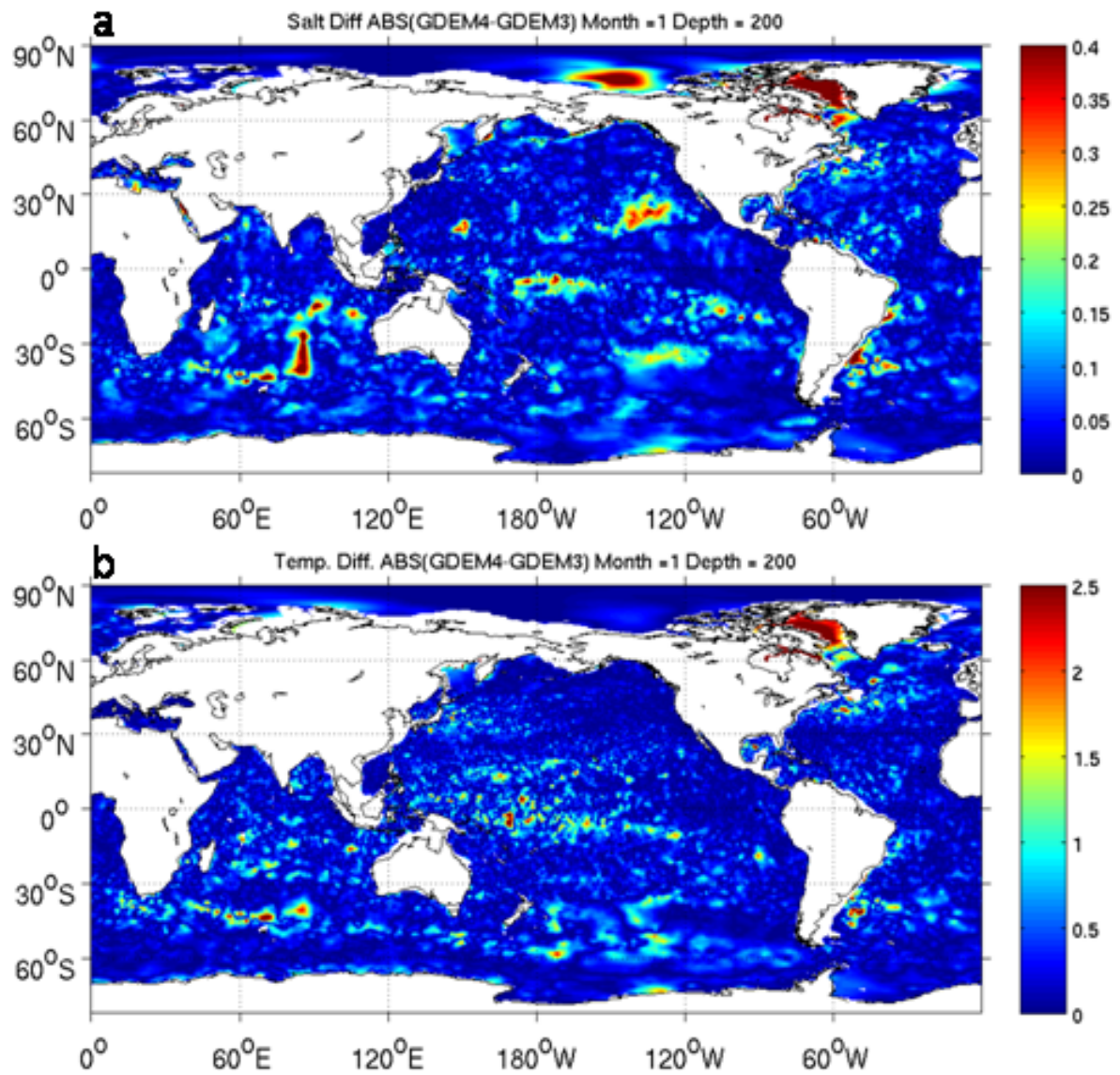


Figure 14 Global maps of the absolute value of the (a) salinity and (b) temperature differences at 200 m depth between the January GDEM4 and GDEM3 climatologies.

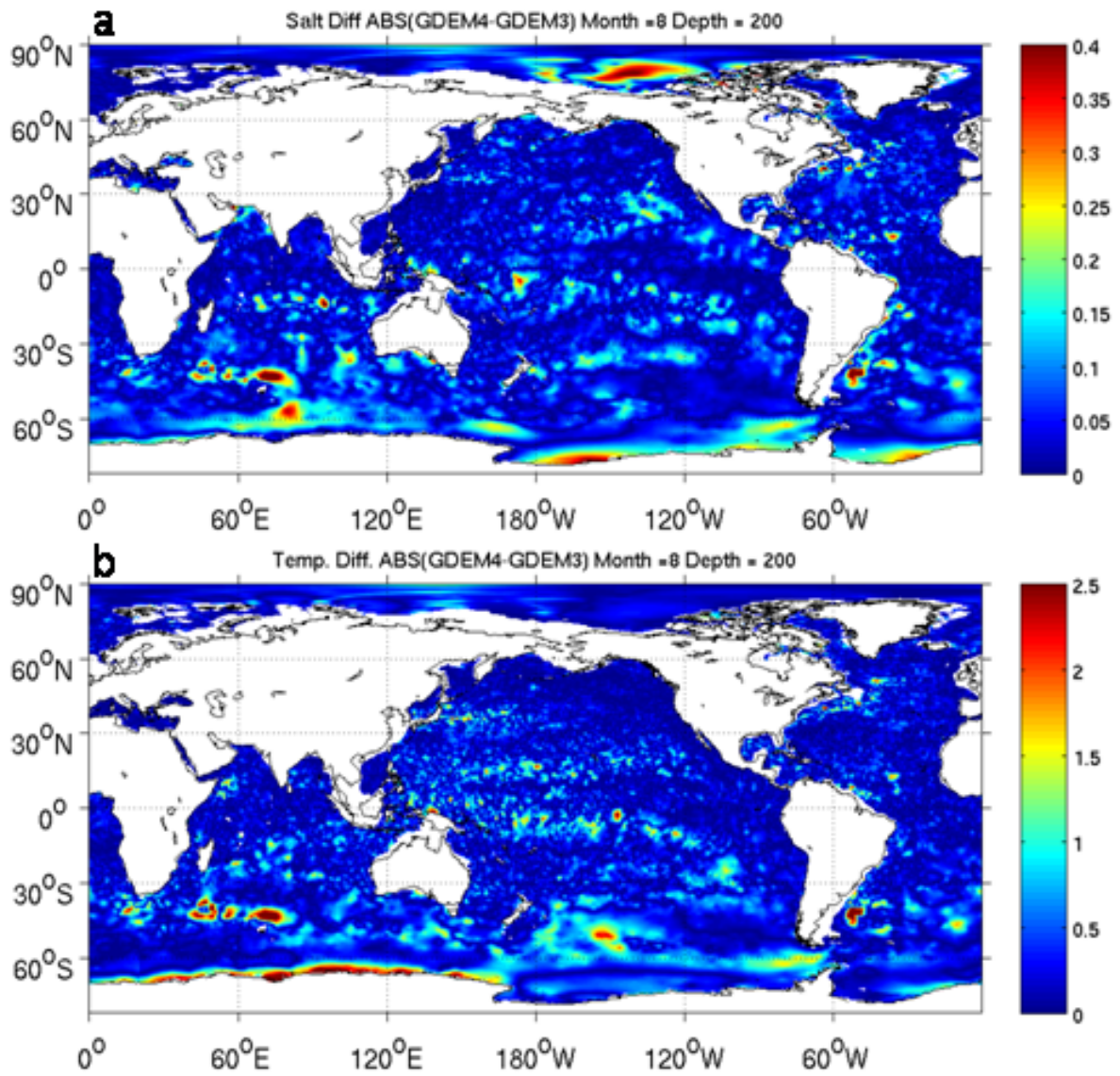


Figure 15 Global maps of the absolute value of the (a) salinity and (b) temperature differences at 200 m depth between the August GDEM4 and GDEM3 climatologies.

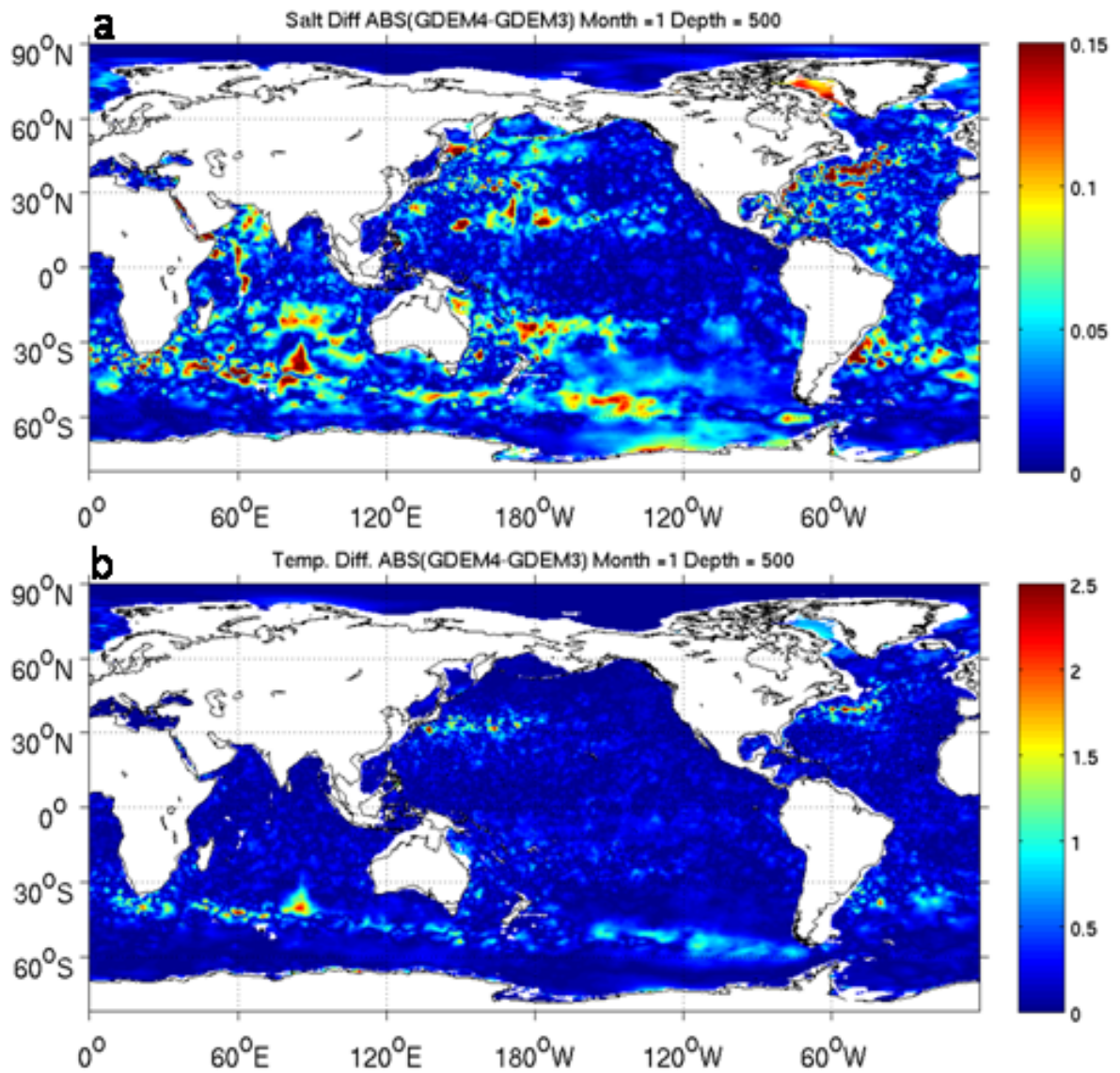


Figure 16 Global maps of the absolute value of the (a) the salinity and (b) temperature differences at 500 m depth between the January GDEM4 and GDEM3 climatologies.

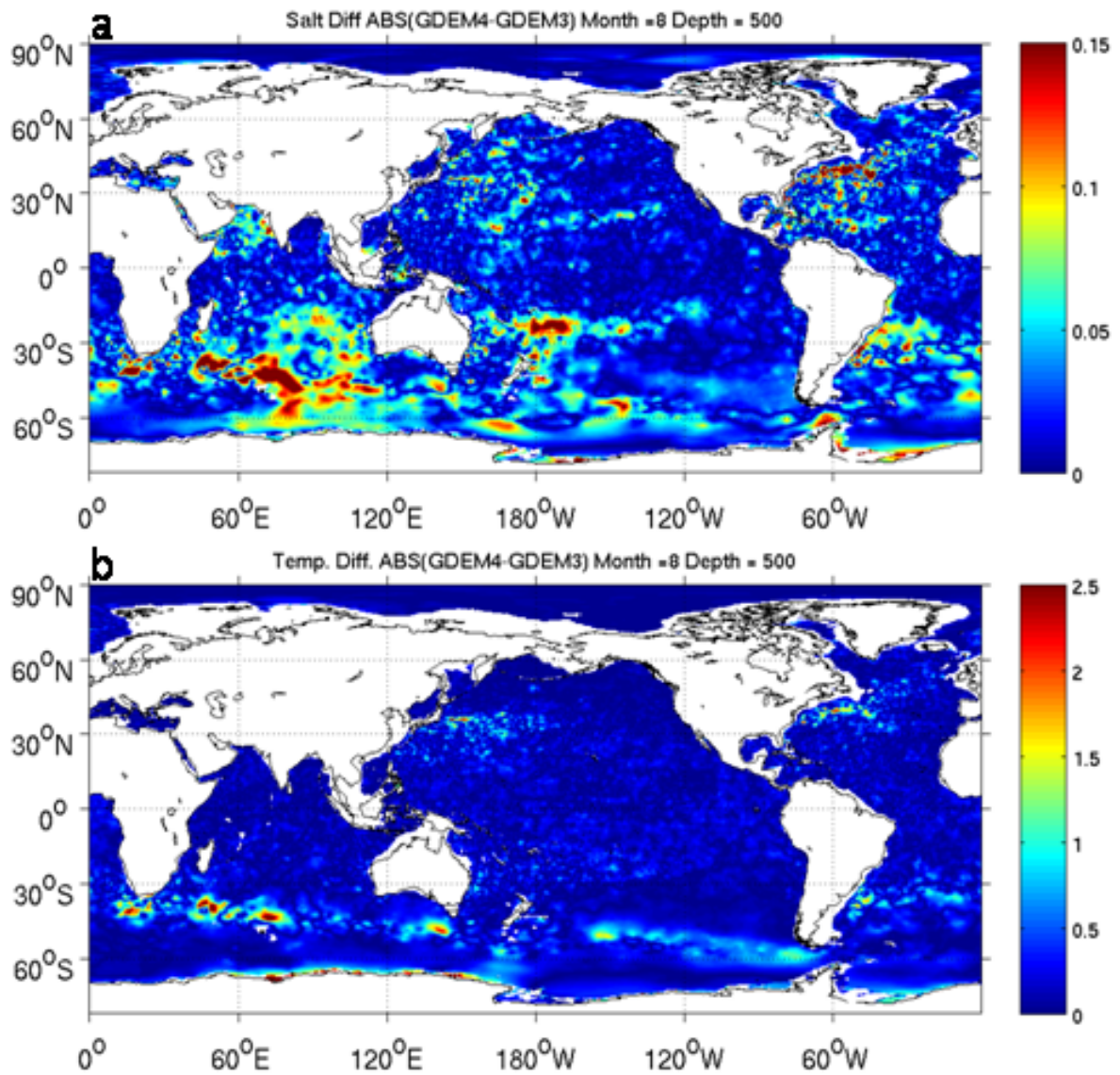


Figure 17 Global maps of the absolute value of the (a) salinity and (b) temperature differences at 500 m depth between the August GDEM4 and GDEM3 climatologies.

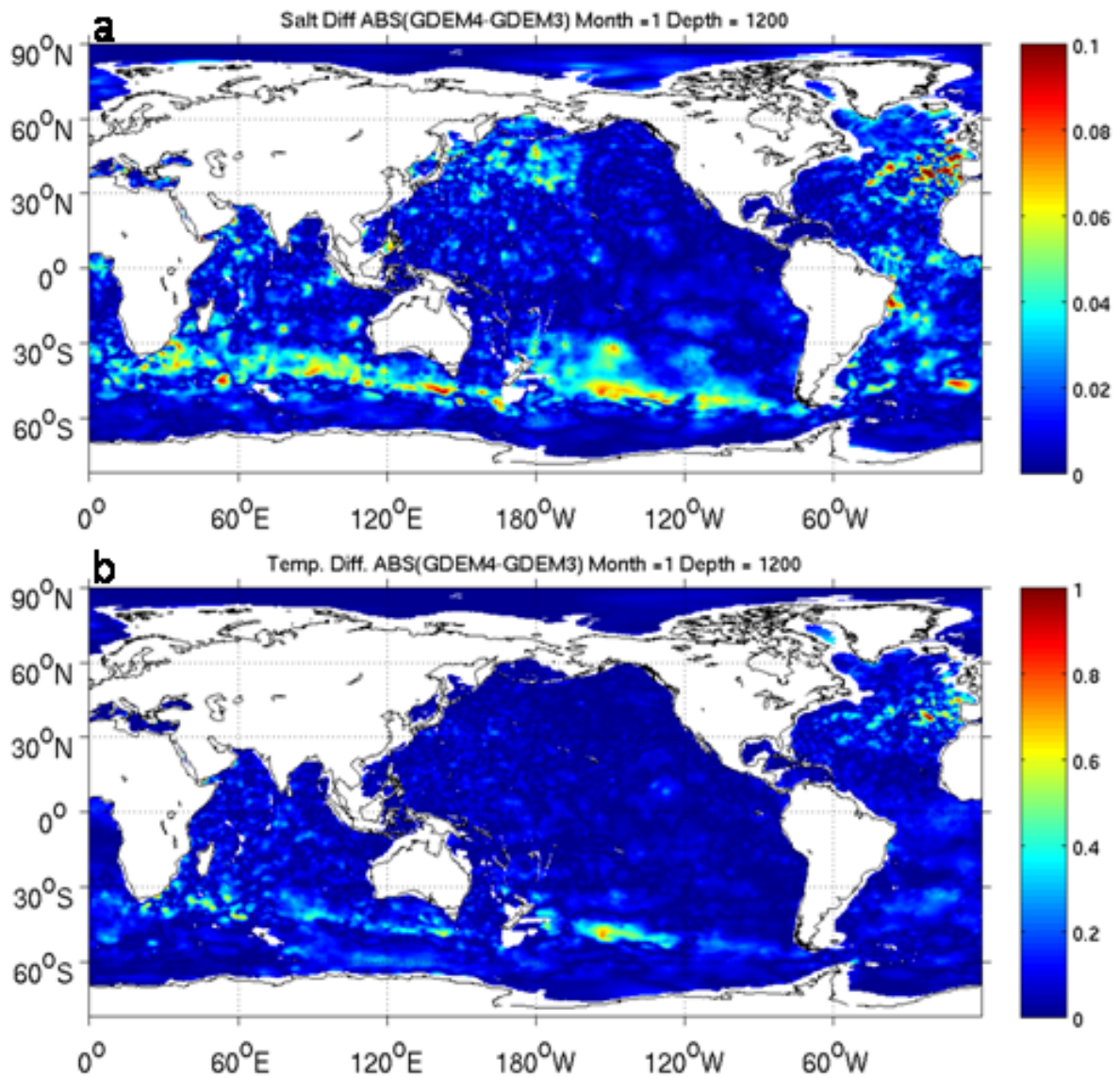


Figure 18 Global maps of the absolute value of the (a) salinity and (b) temperature differences at 1200 m depth between the January GDEM4 and GDEM3 climatologies.

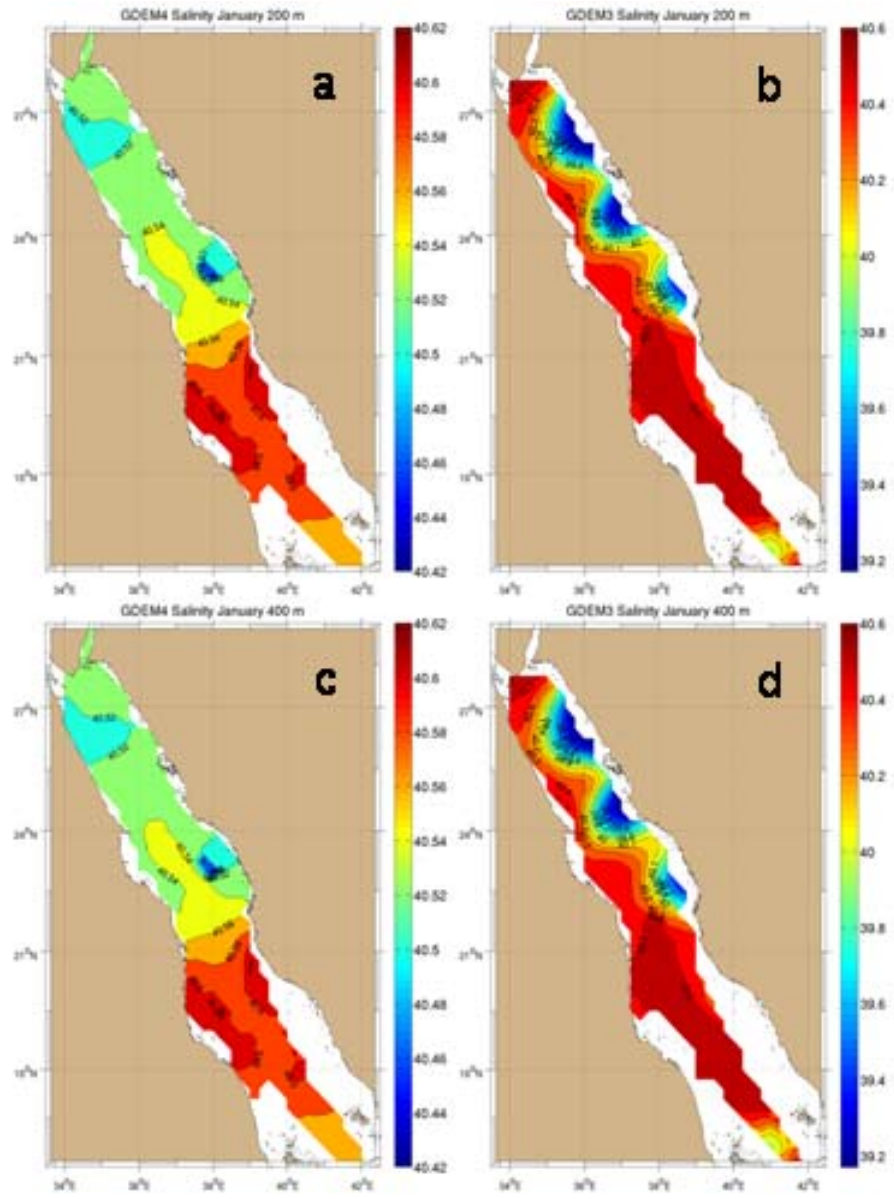


Figure 19 Contour plots of salinity from (a) GDEM4 and (b) GDEM3 at 200 m depth and from (c) GDEM4 and (d) GDEM3 at 400 m depth. The low values of salinity near the coast of Saudi Arabia in the GDEM3 plots (frames b and d) are errors that extend to the bottom.

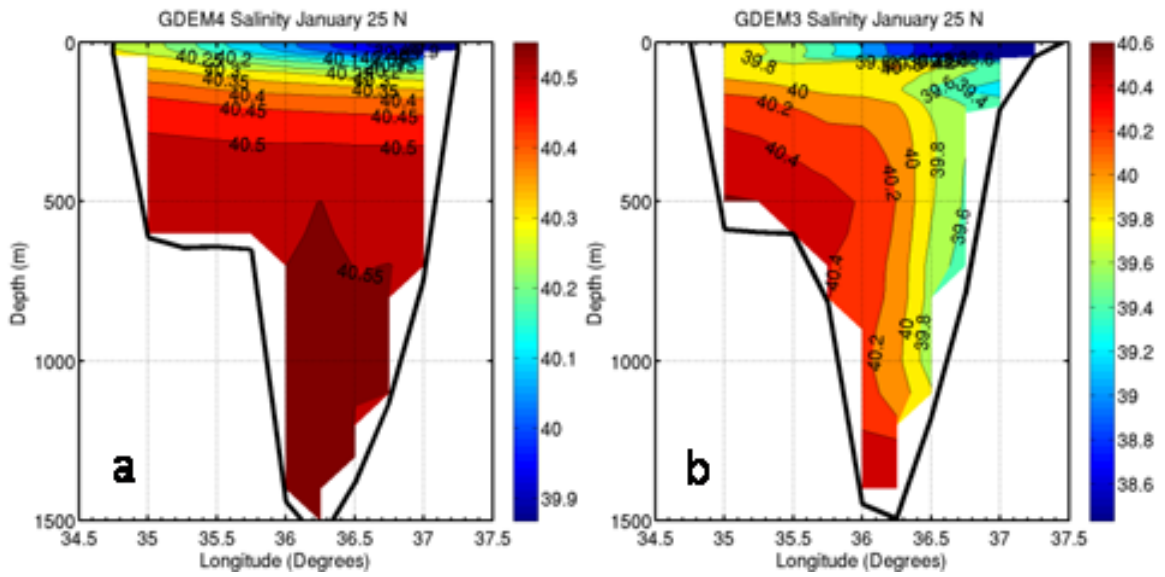


Figure 20 West-to-east vertical sections of salinity in the upper 1500 m along 25° N through the Red Sea from the January (a) GDEM4 and (b) GDEM3 climatologies. The salinity front that freshens toward the east in the GDEM3 plot is due to errors.

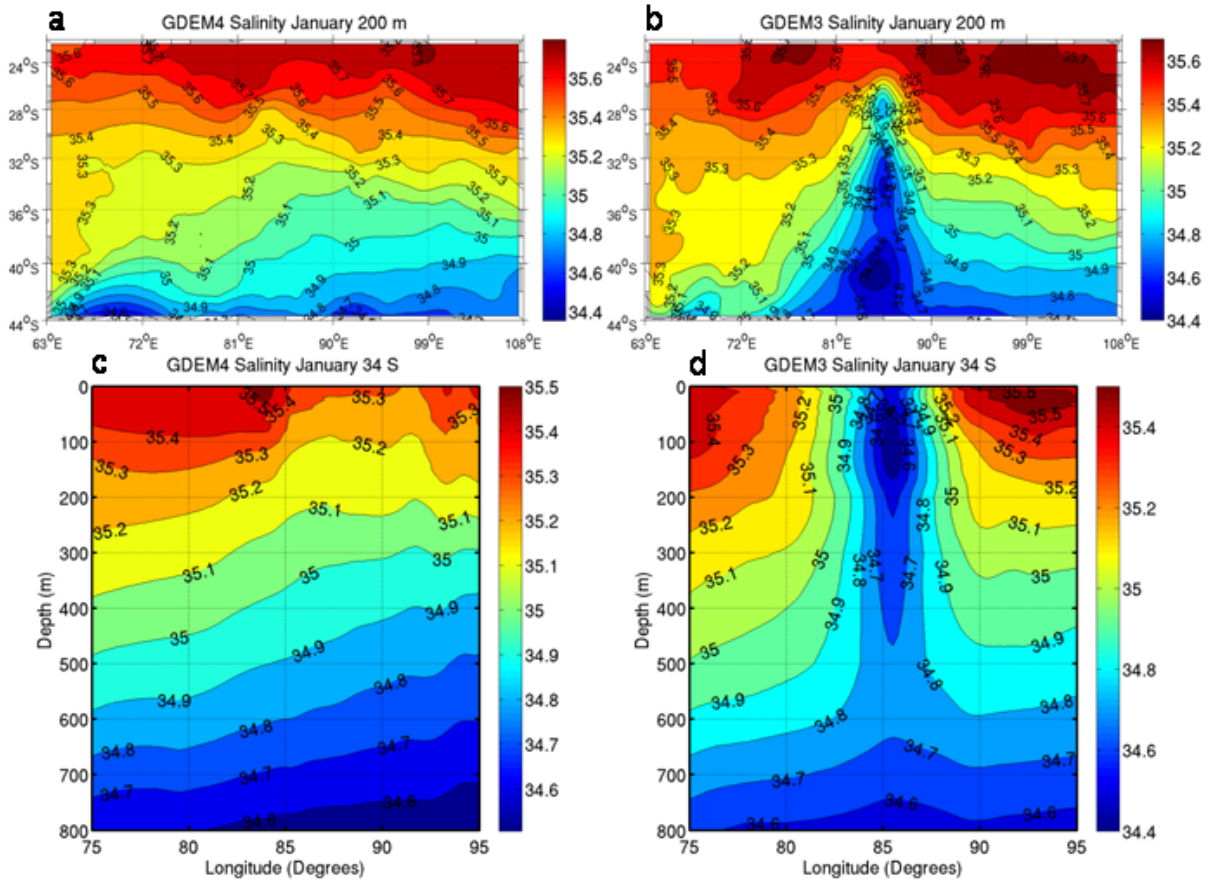


Figure 21 Contour plots of salinity in the southern Indian Ocean near 38° S and 86° E in January from (a) GDEM4 and (b) GDEM3 at 200 m depth, and (c) GDEM4 and (d) GDEM3 on an east-to-west transect along 34° S. Salinity errors are evident in GDEM3 along a north-south line along 85° E extending from the surface to at least 700 m depth.

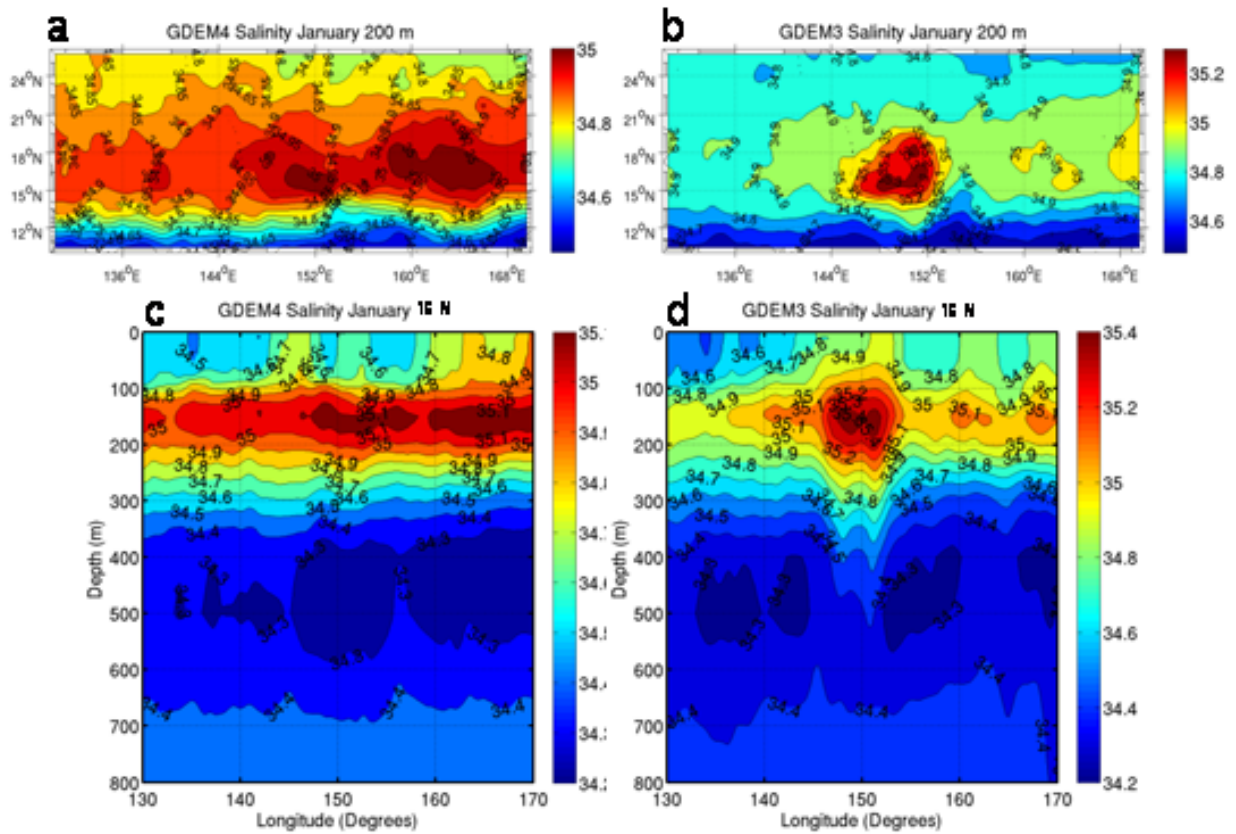


Figure 22 Contour plots of salinity in the eastern Pacific Ocean in the North Equatorial Current near 16° N and 150° E in January from (a) GDEM4 and (b) GDEM3 at 200 m depth, and (c) GDEM4 and (d) GDEM3 on an east-to-west transect along 16° N. Salinity errors are evident in GDEM3 within the bull's eye of high salinity centered near 150 m depth near 150° E.

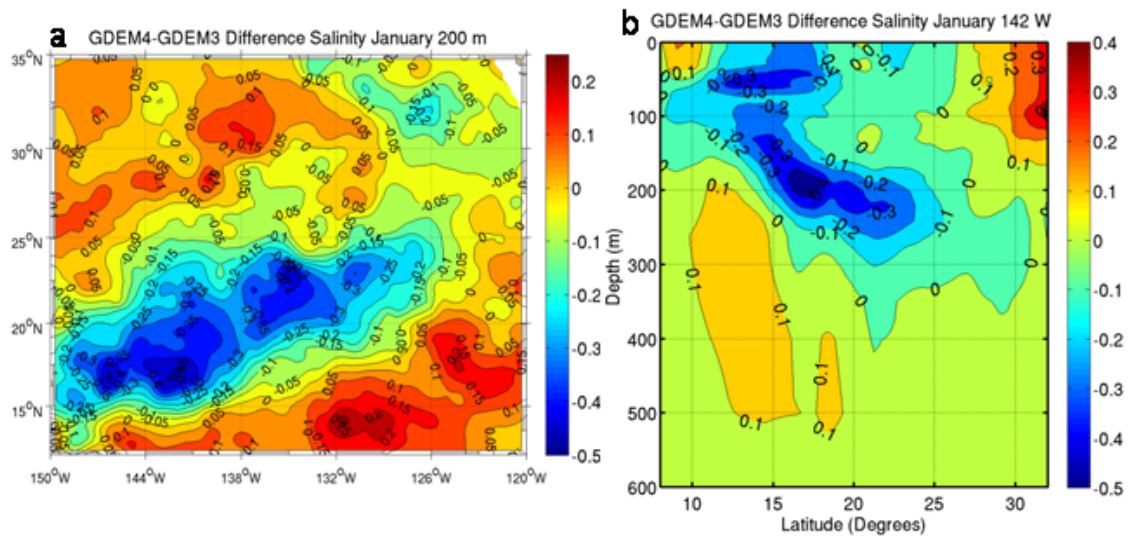


Figure 23 Extended area of large differences in salinity between GDEM4 and GDEM3 east of Mexico in the vicinity of the convergence of the North Equatorial current and the Subtropical Gyre. The map (a) of salinity differences (GDEM4-GDEM3) at 200 m show negative difference up to -0.5 psu are shown to extend downward and toward the north in the south-to-north vertical section (b) along 142° W.

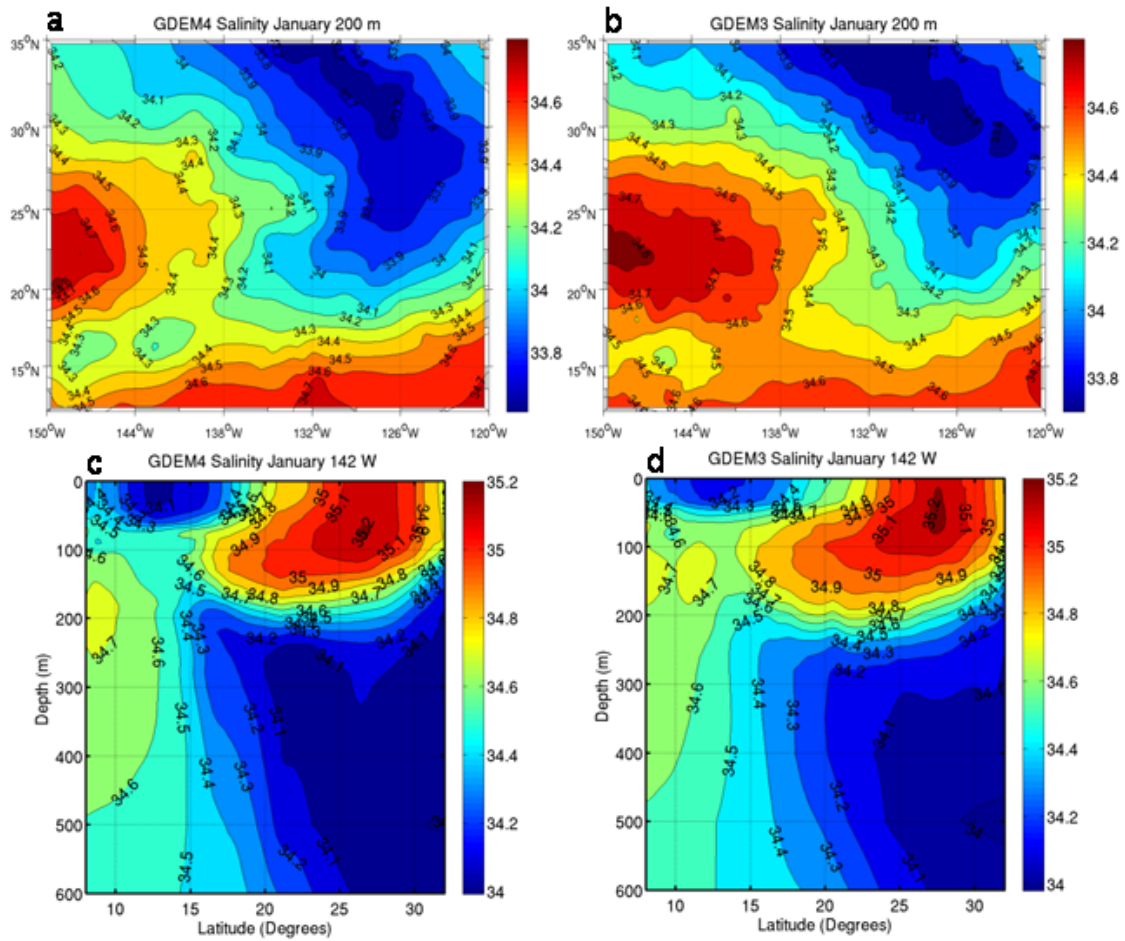


Figure 24 Maps of salinity at 200 m in January from (a) GDEM4 and (b) GDEM3 and vertical sections of salinity in January along the south-to-north vertical section along 142° W from (c) GDEM4 and (d) GDEM3. The large salinity difference between GDEM4 and GDEM3 in this area do not appear to be due to errors in either climatology, but rather to difference in the profile data sets used in their construction and to differences in parameter setting for their gridding algorithms.

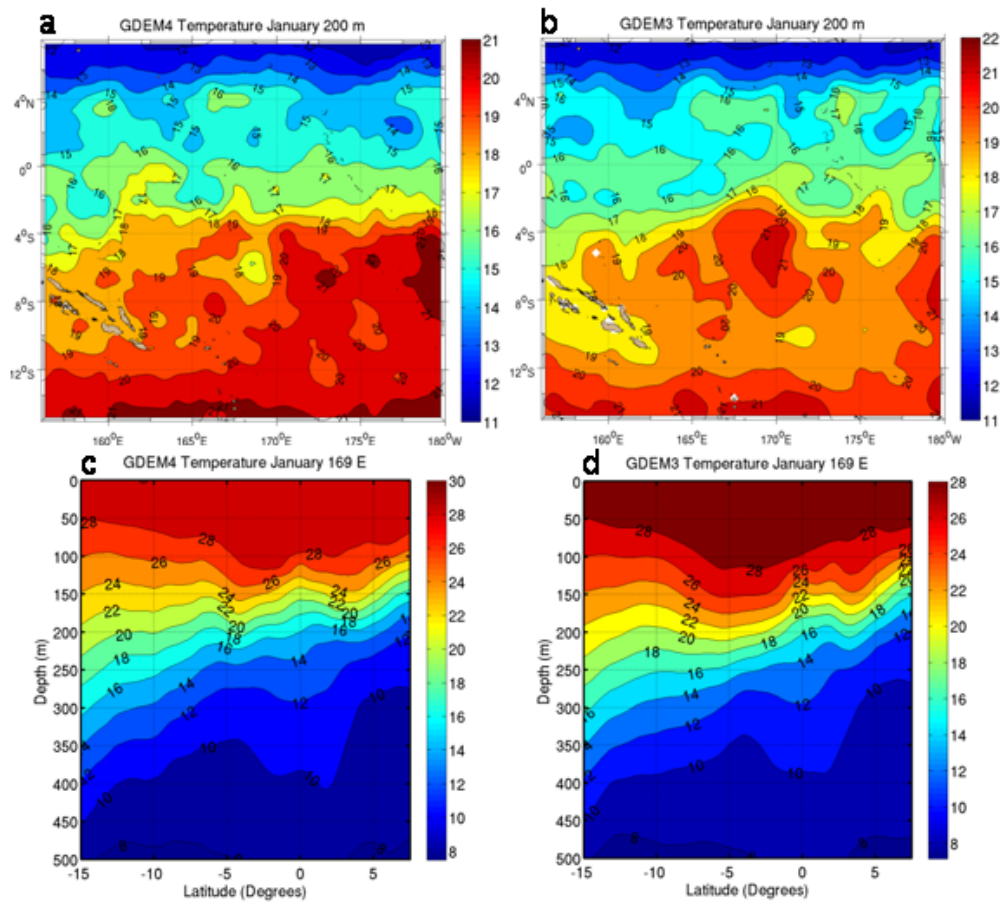


Figure 25 Maps of temperature at 200 m depth in January from (a) GDEM4 and (b) GDEM3 and vertical sections of temperature along 169° E from (c) GDEM4 and (d) GDEM3. Large temperature differences up to 2.5° C at 200 m depth in January at this location as shown in Figure 11b are apparently not due to errors in either climatology, but rather to a combination of large variability in this region and difference in the data set used in the construction of the two climatologies.

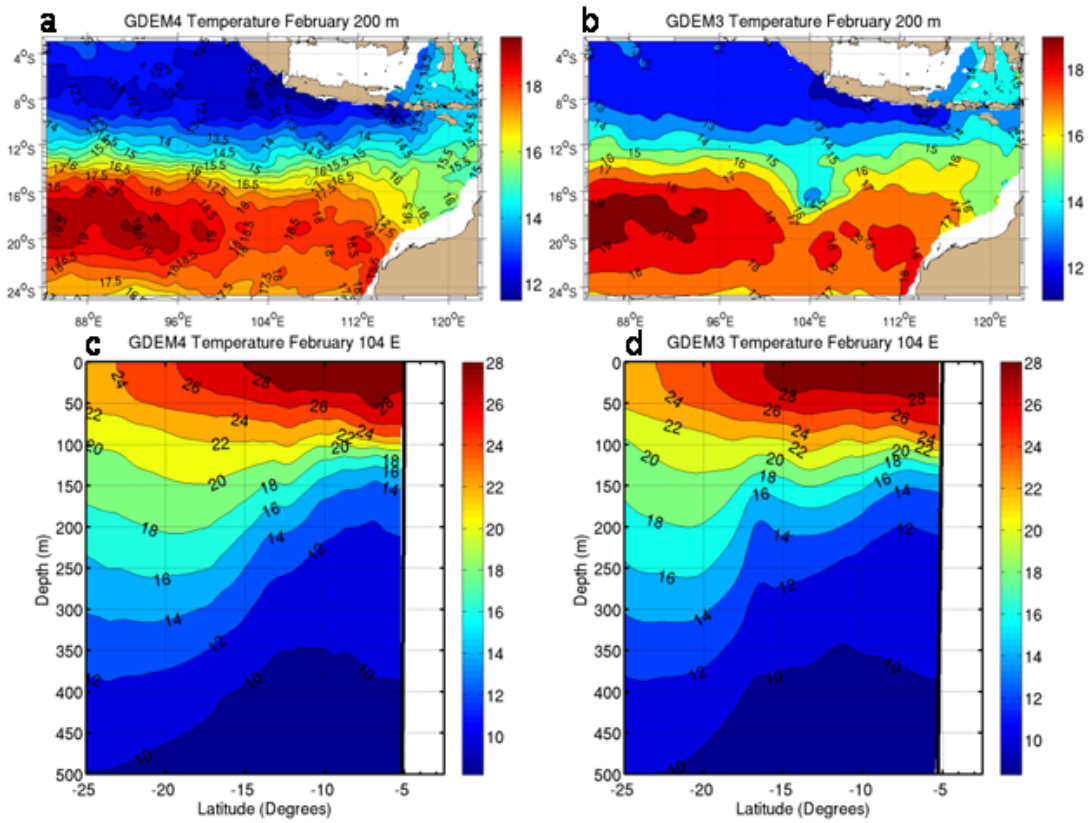


Figure 26 Maps of temperature in the southeastern Indian Ocean at 200 m depth in February from (a) GDEM4 and (b) GDEM3 and vertical sections of temperature along 104° E from (c) GDEM4 and (d) GDEM3. A temperature error in GDEM3 is evident at 16° S and 104° E in the depth range from about 100 m to at least 400 m.

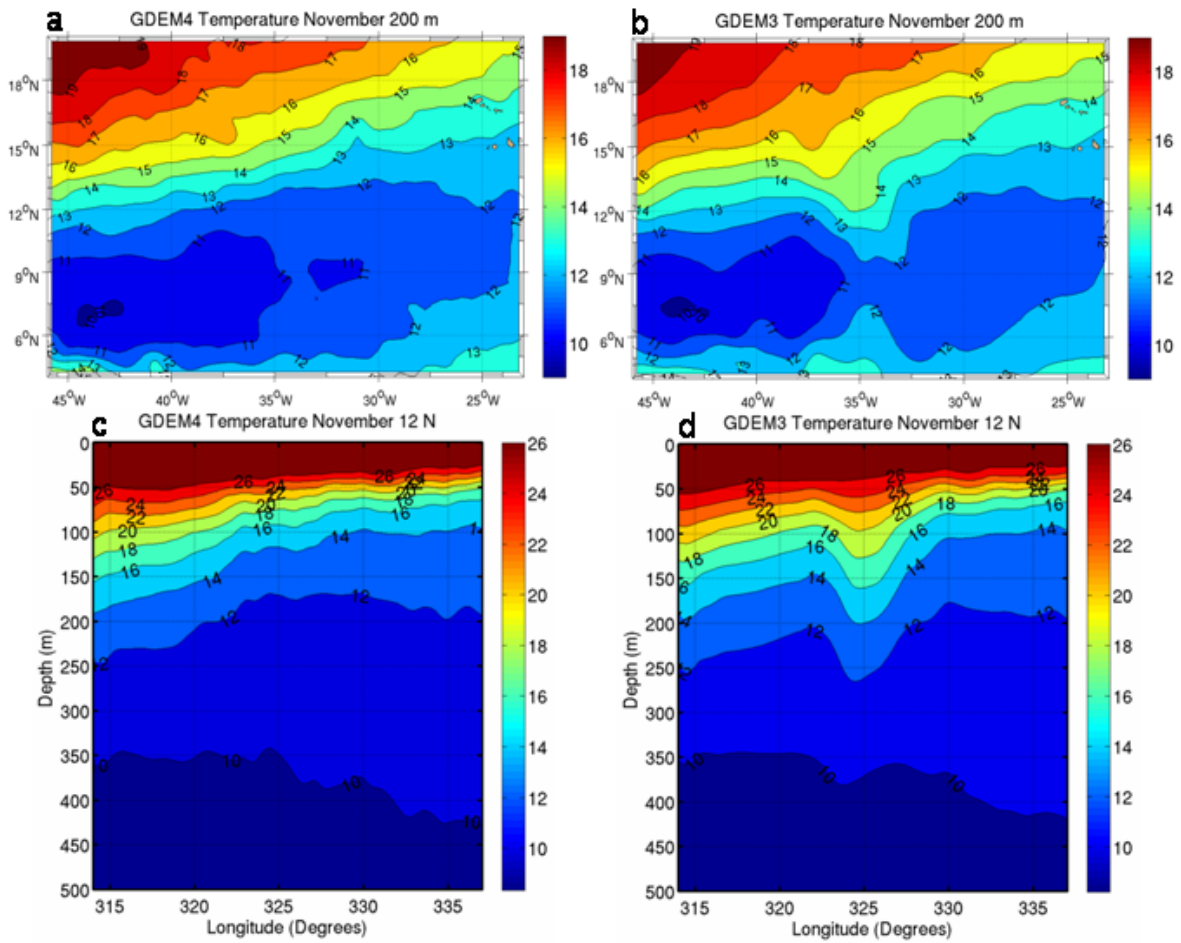


Figure 27 Maps of temperature in the North Atlantic Ocean at 200 m depth in November from (a) GDEM4 and (b) GDEM3 and west-to-east vertical sections of temperature along 12° N from (c) GDEM4 and (d) GDEM3. A temperature error in GDEM3 is evident along a north-south line near 35° W in a depth range from about 75 m to at least 350 m.

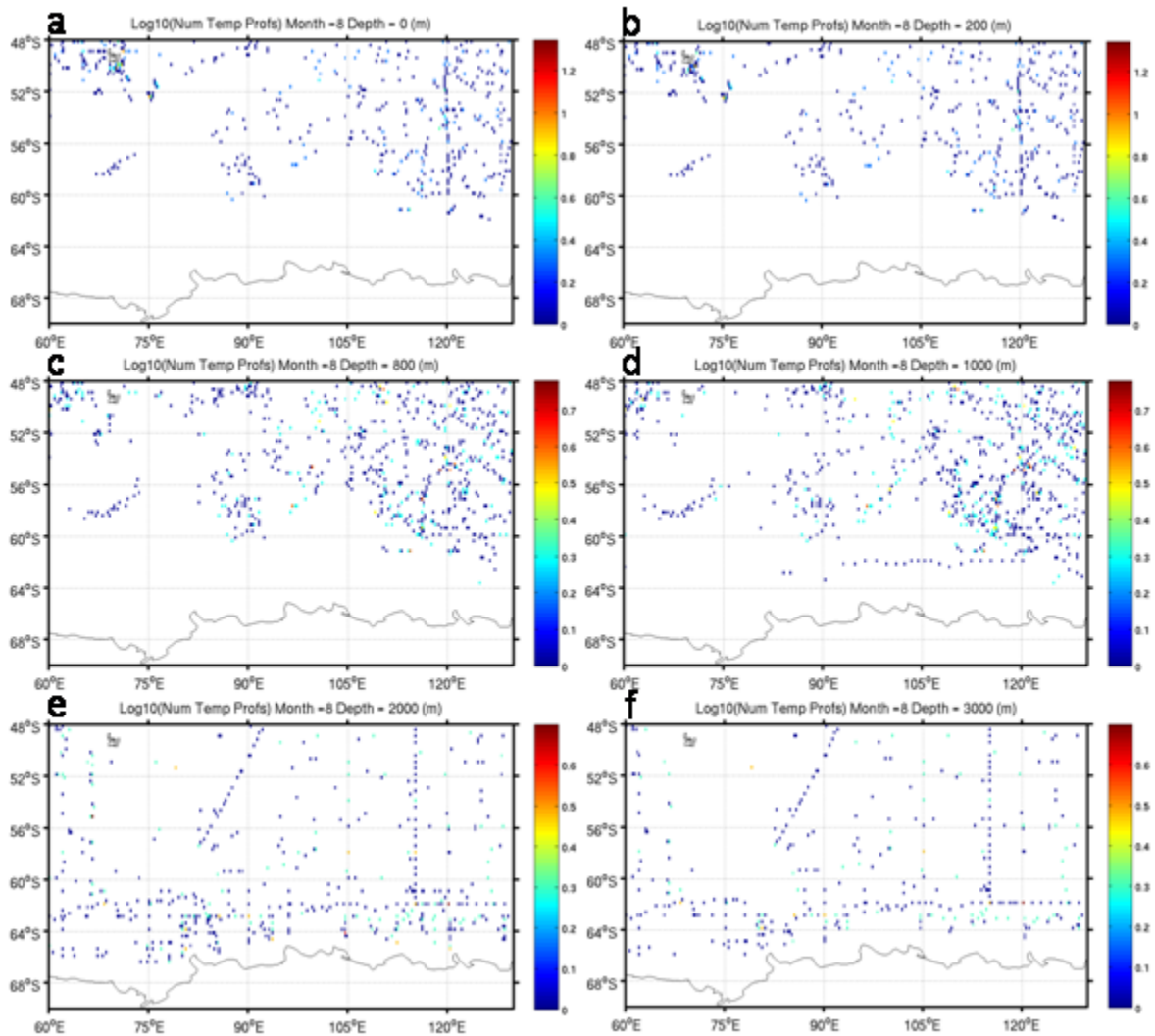


Figure 28 Maps of \log_{10} of the number of temperature observations in the Southern Ocean south of the Indian Ocean down to the Antarctic Continent in each $\frac{1}{4}^\circ \times \frac{1}{4}^\circ$ grid cell used in the construction of the GDEM4 August climatology at (a) the surface, (b) 200 m, (c) 800 m, (d) 1000 m, (e) 2000 m, and (f) 3000 m depth. Grid cells where no observations were available are colored white. The region south of 60° S is devoid of observations from the surface down to at least 800 m depth.

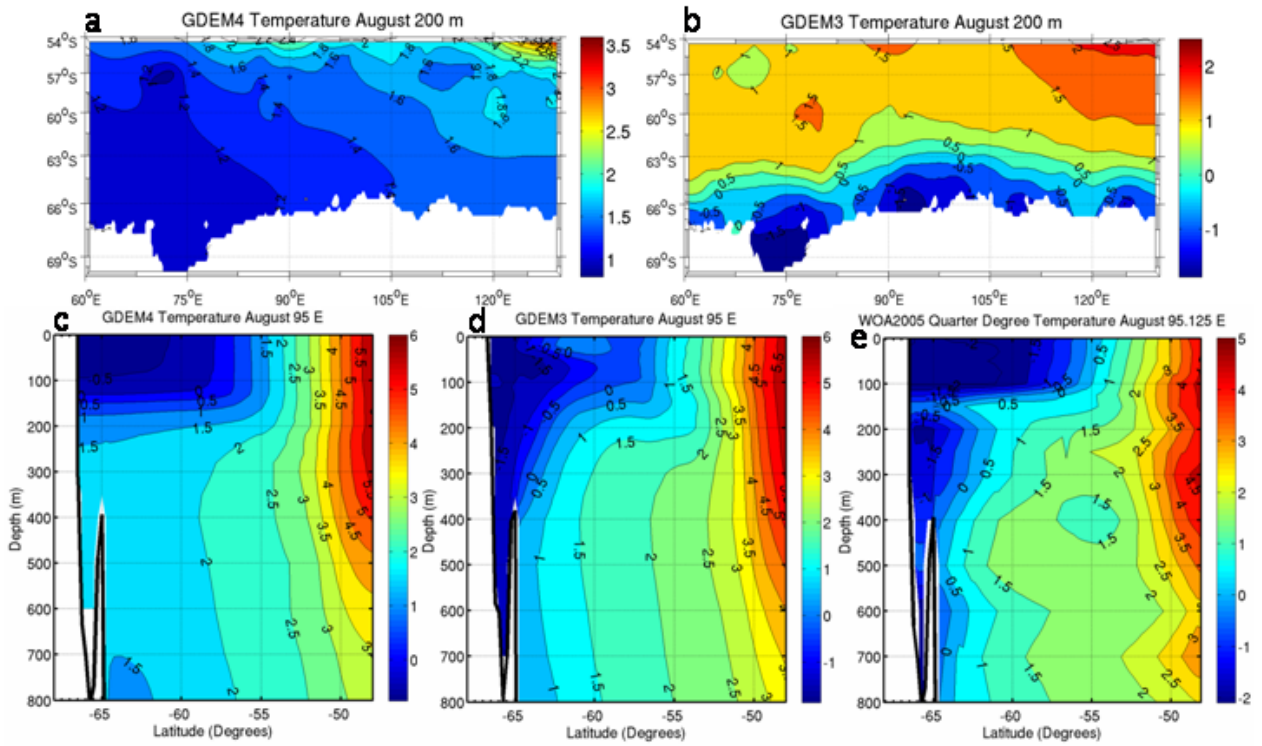


Figure 29 Maps of temperature north of the Antarctic coastline and south of the Indian Ocean in August at 200 m depth contoured from the (a) GDEM4 and (b) GDEM3 climatologies, and vertical sections of temperature in August along 95 E from the Antarctic coast to 48° S in the upper 800 m depth from (c) GDEM4, (d) GDEM3, and (e) WOA2001Q2.

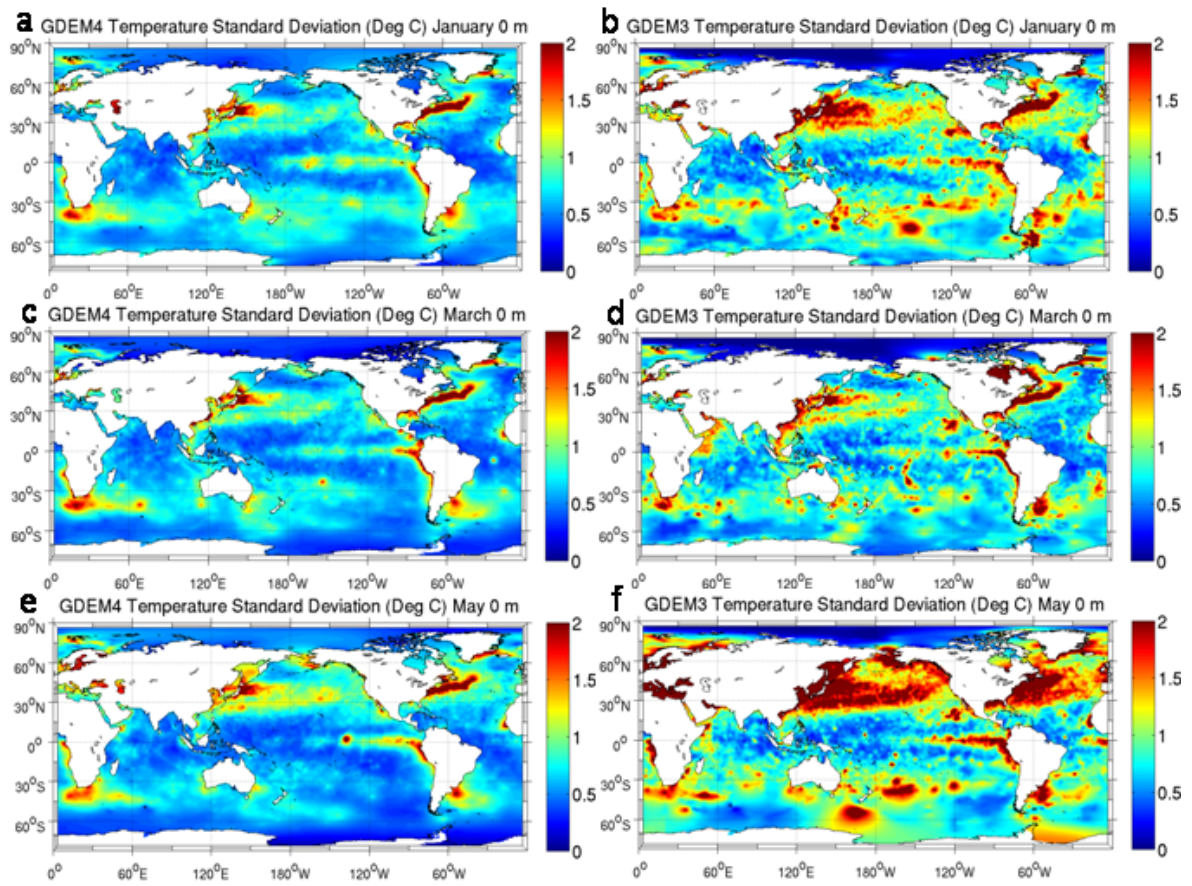


Figure 30 Temperature standard deviation at the surface at bimonthly intervals from GDEM4 (a, c, e, g, i, k) and GDEM3 (b, d, f, h, j, l).

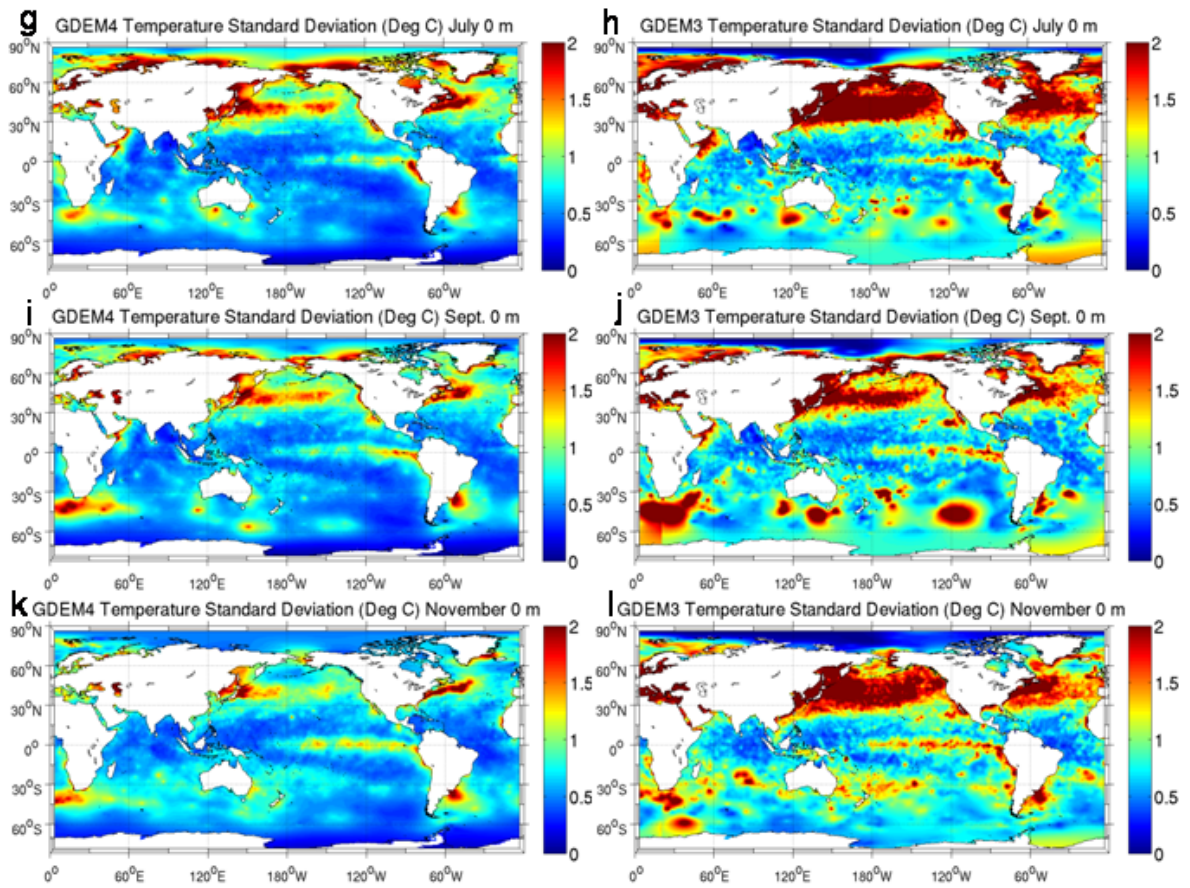


Figure 30 (continued).

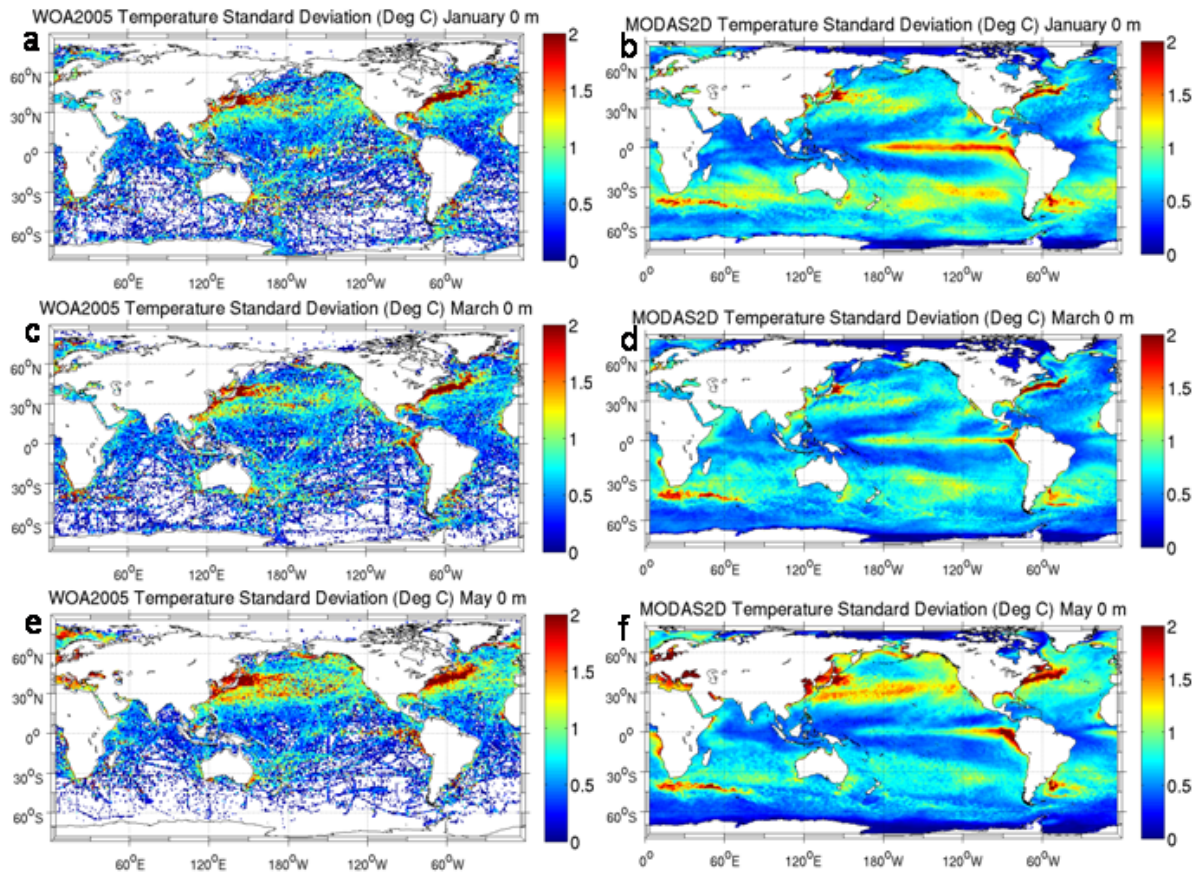


Figure 31 Temperature standard deviation at the surface at bimonthly intervals from the monthly 1°x1°-resolution WOA2005 (a, c, e, g, i, k) and MODAS2D (b, d, f, h, j, l).

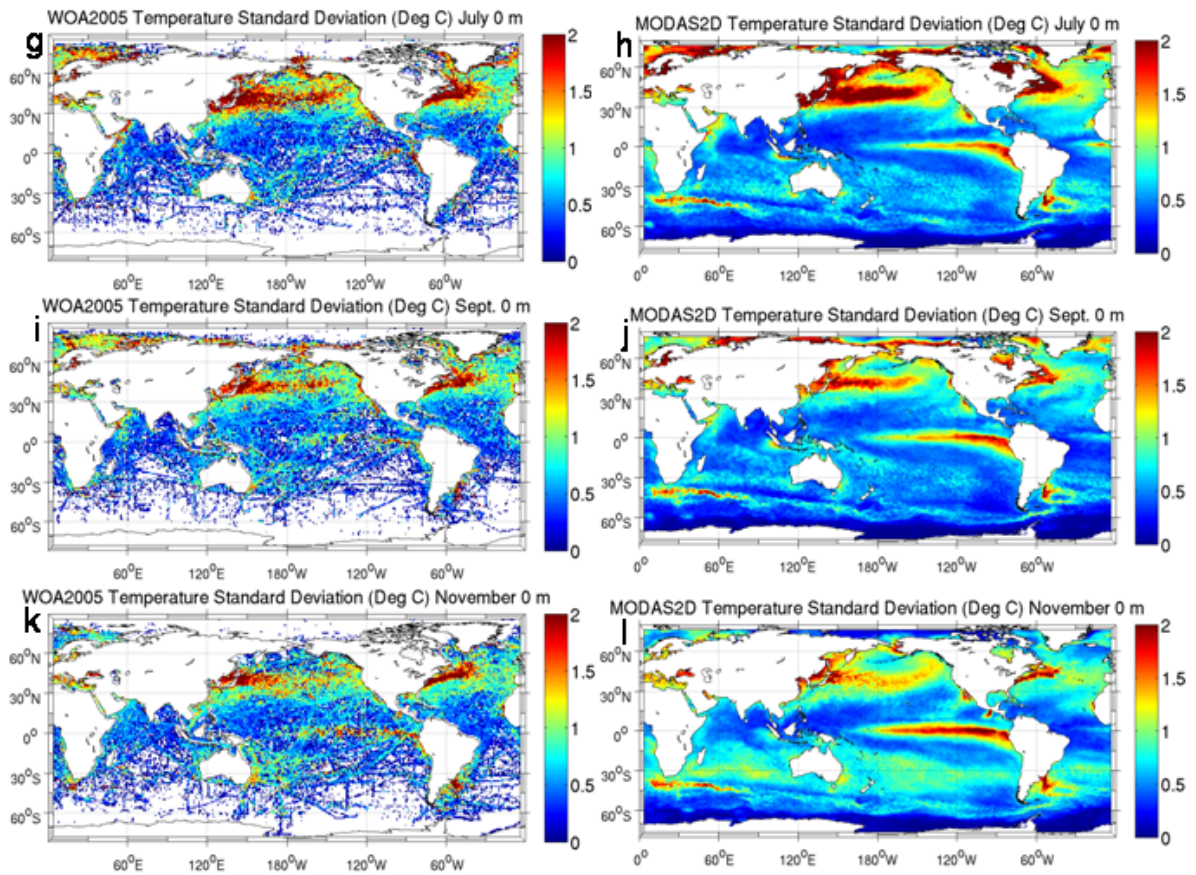


Figure 31 continued

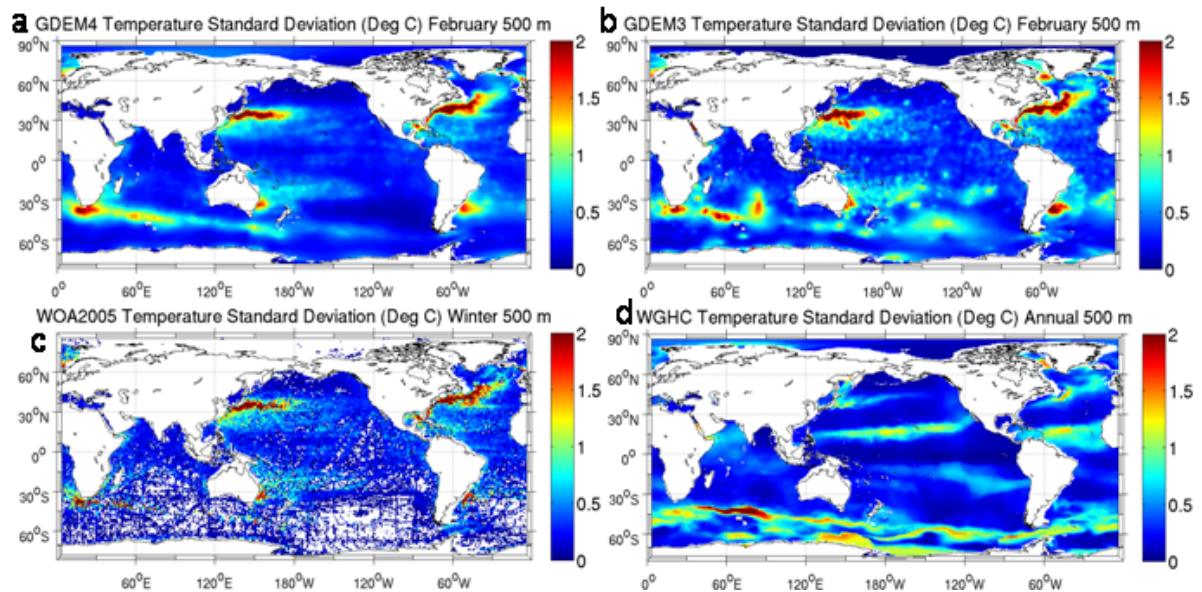


Figure 32 Temperature standard deviation at 500 m depth from (a) GDEM4 in February, (b) GDEM3 in February, (c) the seasonal WOA2005 in winter, and (d) the annual WGHC.

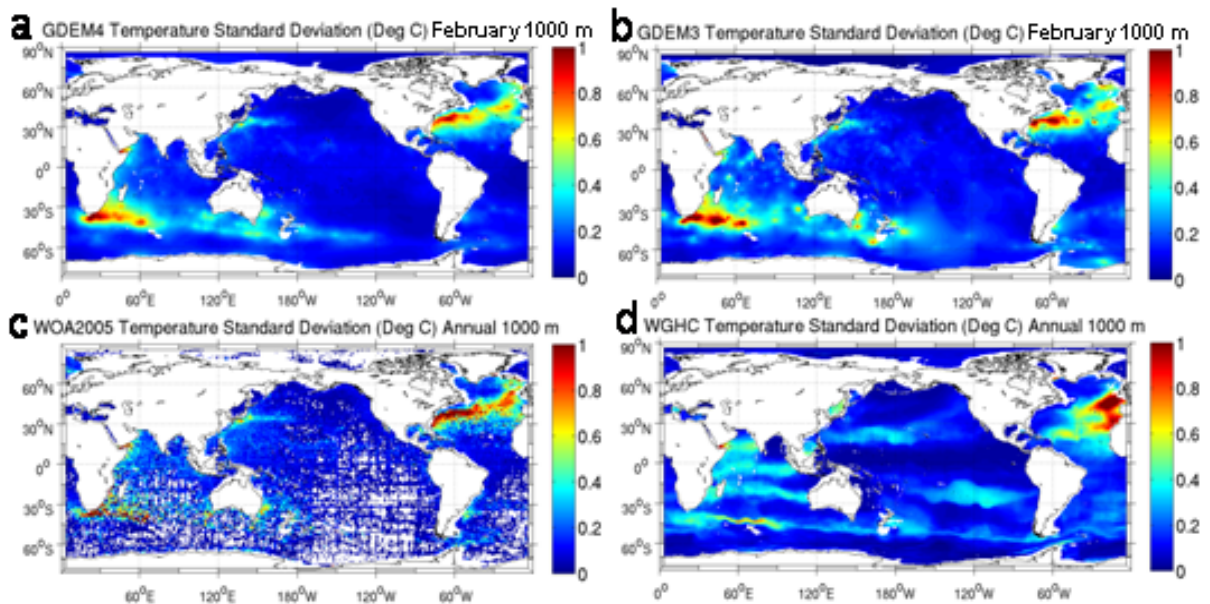


Figure 33 Temperature standard deviation at 1000 m depth from (a) GDEM4, (b) GDEM3, (c) the annual WOA2006, and (d) WGHC. The GDEM4 and GDEM3 temperature standard deviations are from the February climatology, but both climatologies are constructed using a 4-month span of profile observations at 1000 m depth.

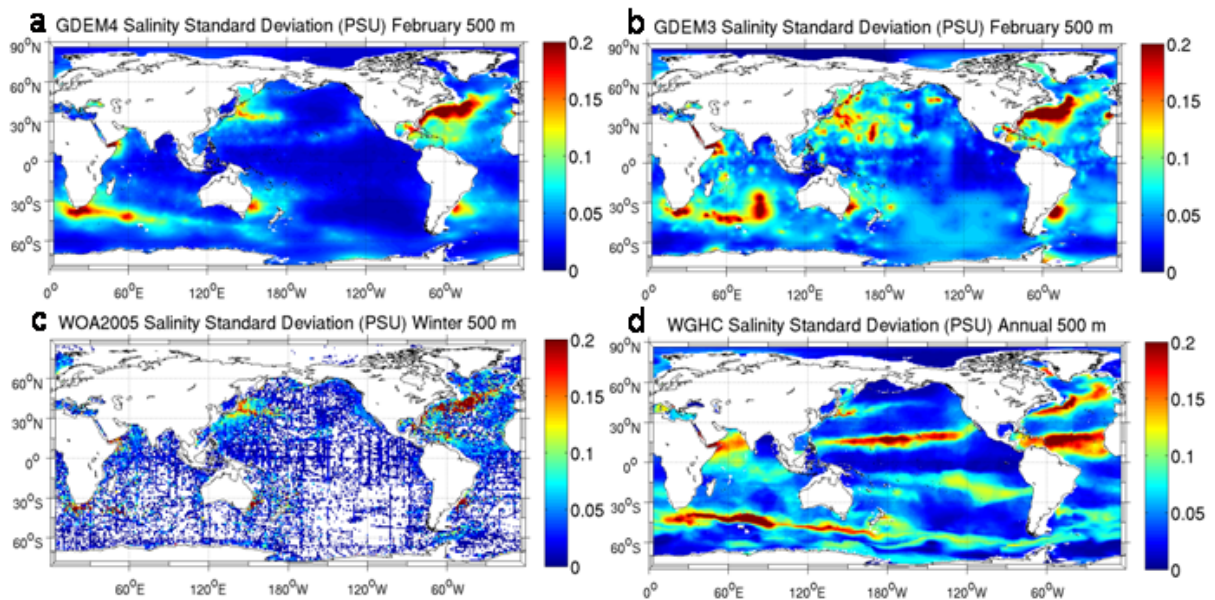


Figure 34 Salinity standard deviation at 500 m depth from (a) GDEM4 in February, (b) GDEM3 in February, (c) the seasonal WOA2005 in winter, and (d) the annual WGHC

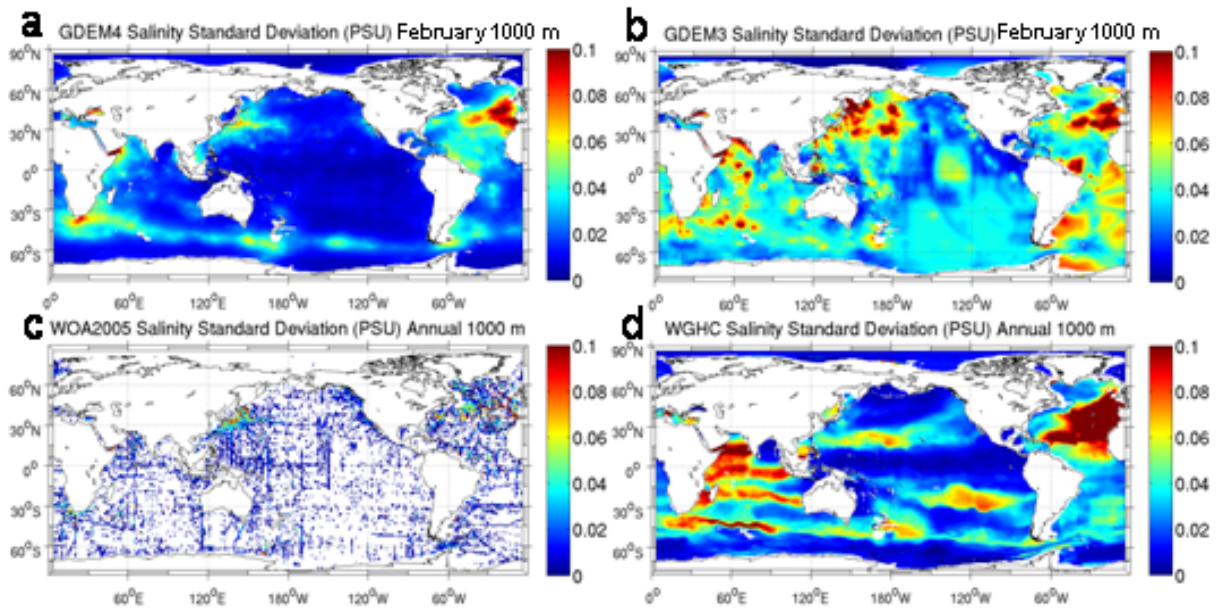
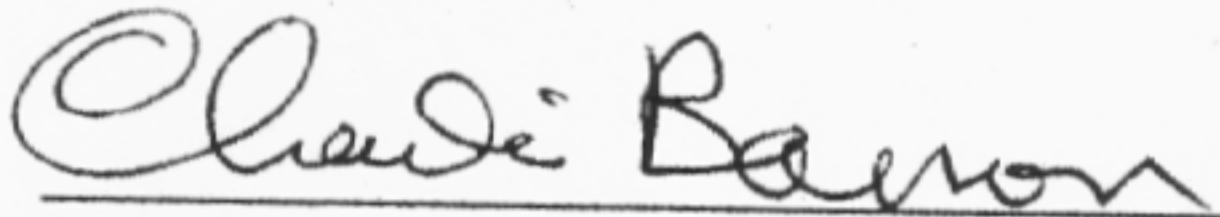


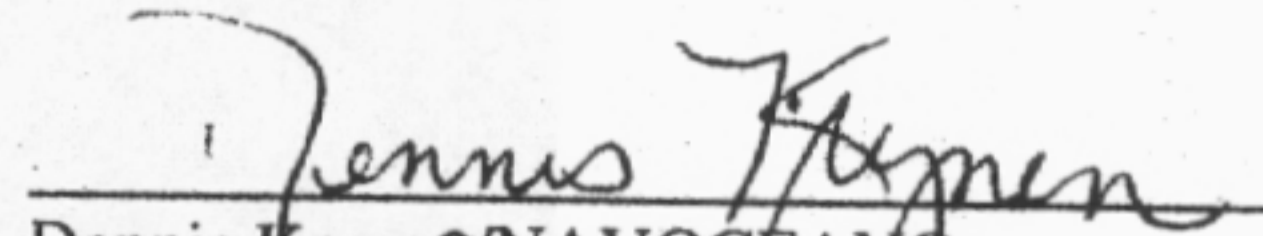
Figure 35 Salinity standard deviation at 1000 m depth from (a) GDEM4, (b) GDEM3, (c) the annual WOA2006, and (d) WGHC. The GDEM4 and GDEM3 temperature standard deviations are from the February climatology, but both climatologies are constructed using a 4-month span of profile observations at 1000 m depth.

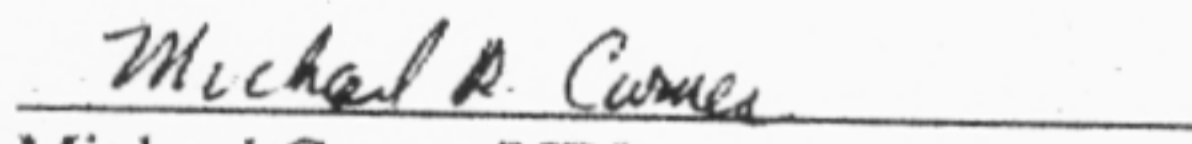
19. FINAL ACCEPTANCE:

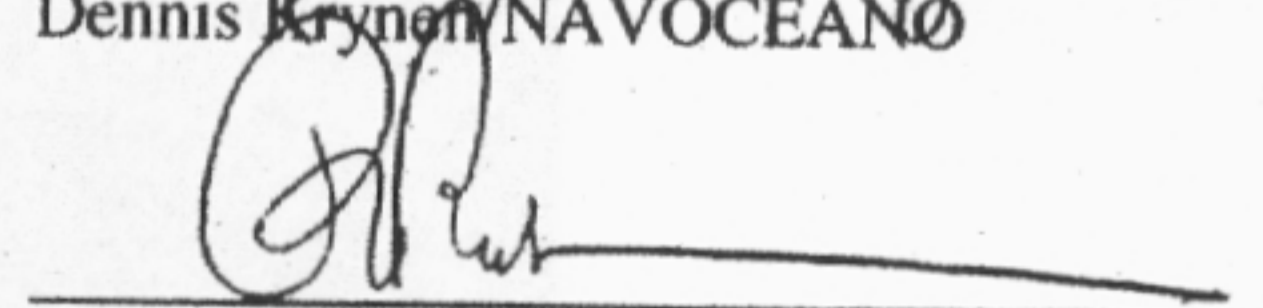
By signing below, the requisite authority attests that the VTR and all deliverables were completed satisfactorily and the transitioned system is operating nominally providing the capability proposed to the best of his or her knowledge.

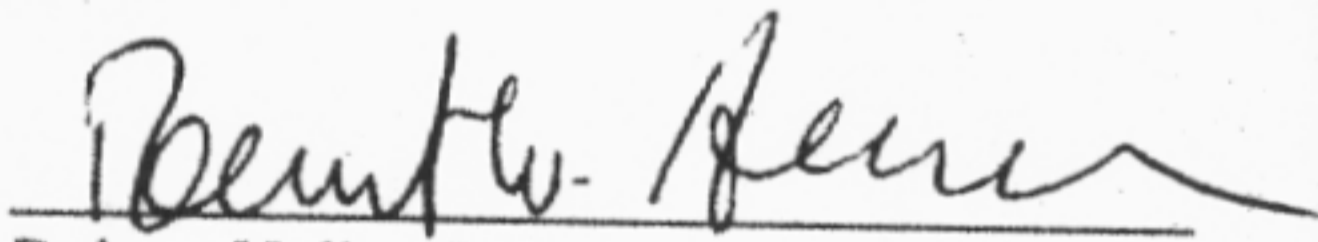
Validation Test Panel:

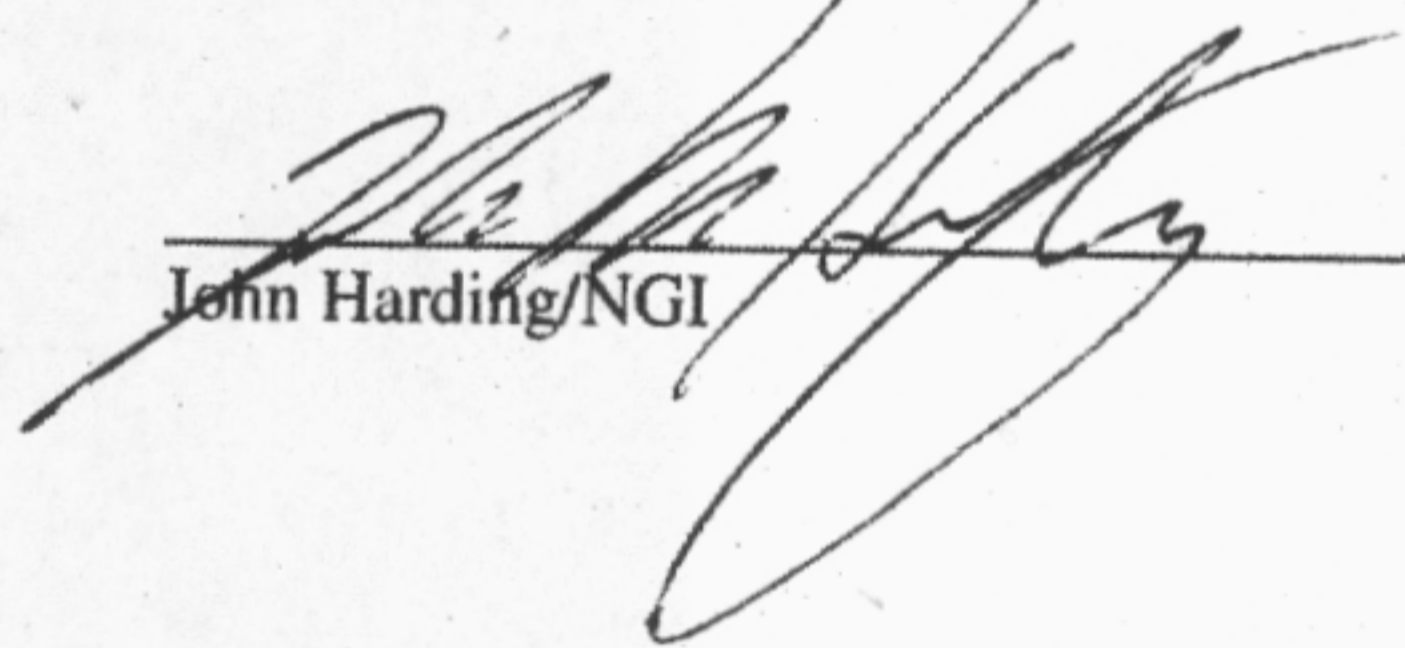

Charlie Barron/NRL


Dennis Krynen/NAVOCEANO

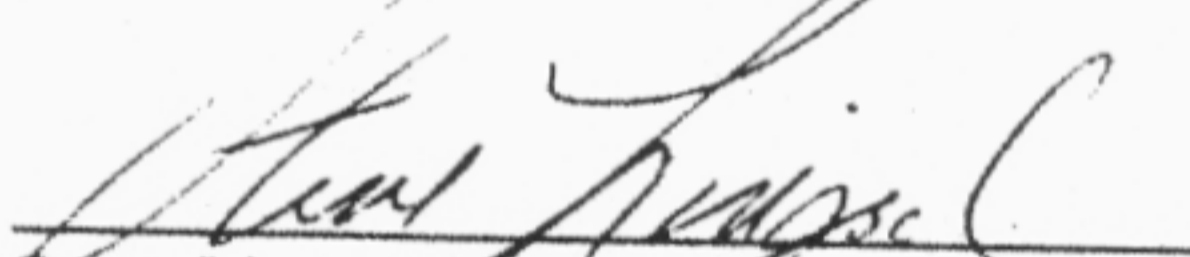

Michael Carnes/NRL

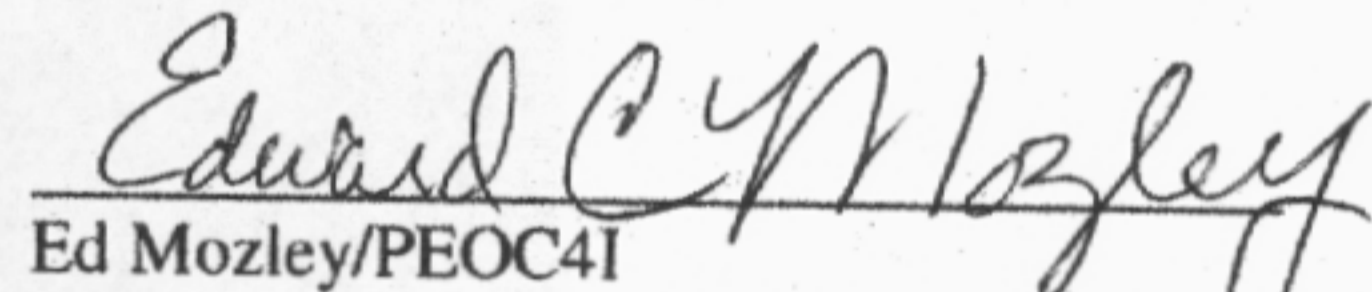

Frank Bub/NAVOCEANO

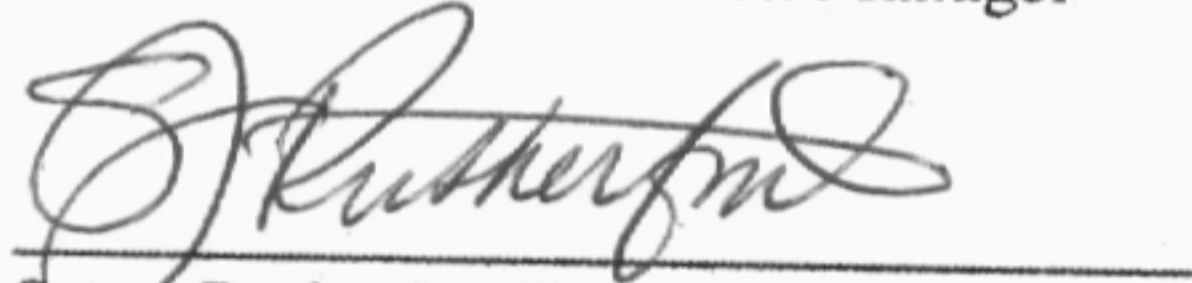

Robert Helber/NRL

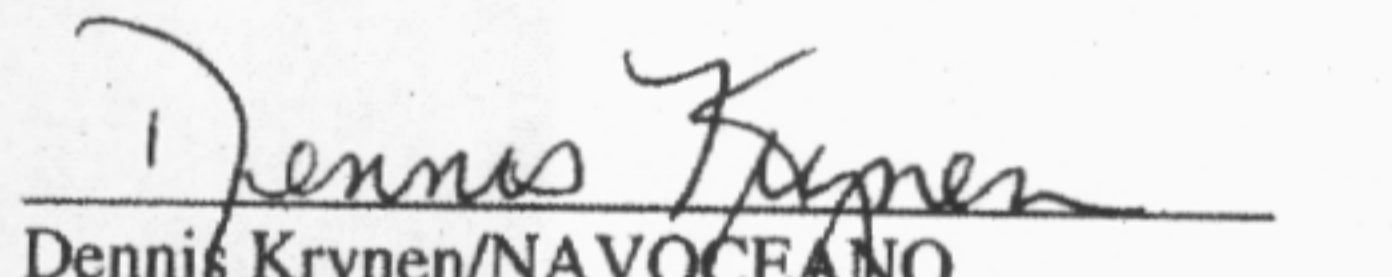

John Harding/NGI

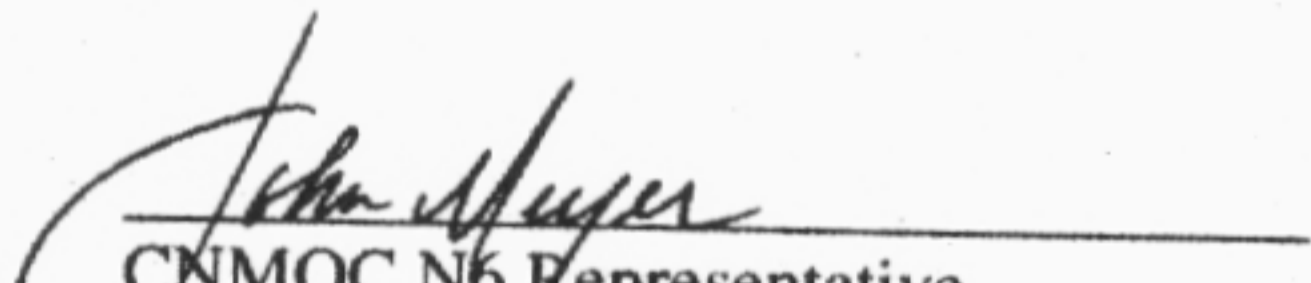
CNMOC/Transition Representatives:


Steve Lingsch/CNMOC
CNMOC R&D Transition Manager


Ed Mozley/PEOC4I
Program Office Acquisition Project Manager


Steve Rutherford/OPNAV
Funding Resource Officer


Dennis Krynen/NAVOCEANO
Operational Transition Partner Representative


CNMOC N6 Representative
Information Architecture Department

